International Review of
Chemical Engineering
Rapid Communications
(IRECHE)

Contents

Praise Worthy Prize

Copyright © 2014 Praise Worthy Prize S.r.l. - All rights reserved

Praise Worthy Prize

International Review of Chemical Engineering (I.RE.CH.E.), Vol. 6, N. 4
ISSN 2035-1755 *July 2014*

Studies on Performance Characteristics of Diverging – Converging Fluidized Bed Biofilm Reactor with Special Reference to Lactic Acid Synthesis from Molasses and Cheese Whey

C. M. Narayanan, Ananya Basak, Arpita Saha, Soni Jha

Abstract – *Attempts have been made to study the synthesis of lactic acid by microbial fermentation of molasses and cheese whey permeate in a fluidized bed bioreactor of diverging – converging geometry. The reactor core consists of support particles (polymer beads) each surrounded by a thin film of microbial solution (Enterococcus Faecalis culture in case of molasses and a culture of Lactobacillus helveticus in case of cheese whey permeate) and these particle – biofilm aggregates remain fluidized in the ascending stream of the feed solution. The core is composed of three segments each of length L_S and the feed solution is admitted from the bottom at the minimum cross – section. The angle of convergence / divergence is maintained constant at 5^0 throughout the length of the column. The performance of the bioreactor is analysed mathematically by developing a simulation model that assumes dispersed flow through the reactor, with continuous change of superficial fluid velocity along the length (height) of the reactor column.*

The performance equations are solved using a specially developed numerical algorithm NUMCM that involves a modified form of Runge – Kutta method. Solution using line successive over – relaxation (SOR) method has also been attempted. Extensive experimental data have also been collected using a laboratory bioreactor of proposed geometry. Excellent agreement has been observed between results computed using the software package developed and the experimental data compiled (maximum deviation = $\mp$ 10%). It has also been observed that the bioreactor of proposed design provides distinctly superior performance (provides 20 to 25 % higher fractional conversion of substrate) when operating at the same feed flow rate and feed inlet concentration as compared to a conventional fluidized bed of same reactor volume. ***Copyright © 2014 Praise Worthy Prize S.r.l. - All rights reserved.***

Keywords*: Fluidized Bed Bioreactor, Diverging – Converging Geometry, Lactic Acid Synthesis, Software Development*

Nomenclature

Ar_m	Modified Archimedes number, dimensionless
C_D	Drag coefficient, dimensionless
$C_S(z)$	Substrate concentration at any cross-section z, gm/L
C_{S0}	Substrate concentration in feed solution, gm/L
C_{Se}	Substrate concentration in product solution, gm/L
d_P	Diameter of support particle, m
d_{Pm}	Diameter of particle-biofilm aggregate, m
$D(z)$	Diameter of the bioreactor at any cross-section z, m
D_1	Minimum diameter of the bioreactor, m
D_2	Maximum diameter of the bioreactor, m
D_e	Effective diffusivity of substrate into biofilm, m^2/s
D_L	Axial dispersion coefficient, m^2/s
D_V	Volumetric diameter of diverging – converging column, m
f	Volume fraction of biofilm in particle-biofilm aggregate, dimensionless
K_S	Half velocity constant, gm/L
L^*	Characteristic length, m
L_S	Length of each segment of the bioreactor, m
L_f	Total height of the fluidized bed (reaction zone), m
Q_0	Substrate flow rate , m^3/s
$(-r_S)_{(int)}$	Intrinsic rate of reaction, gm/(Ls)
Re_{mf}	Reynolds number at minimum fluidization, dimensionless
Re_P	Particle Reynolds Number, dimensionless
U_{mf}	Minimum fluidization velocity, m/s
$U_{SUP}(z)$	Superficial velocity of substrate solution at any z, m/s
V_t	Terminal free settling velocity of particle-biofilm aggregate, m/s

Copyright © 2014 Praise Worthy Prize S.r.l. - All rights reserved

x_f	Cell mass concentration in biofilm, gm/L
Y	Overall yield coefficient for cell mass production, dimensionless
z	Axial co-ordinate
α	Fractional conversion of substrate attained, dimension less
β(z)	Parameter defined in equation (24), dimensionless
θ	Angle of convergence / divergence, degrees
δ	Biofilm thickness, m
ρ_{Sm}	Density of particle-biofilm aggregate, kg/m^3
ρ_m	Density of microbial solution, kg/m^3
ρ_S	Density of support particle, kg/m^3
ρ_f	Density of substrate solution, kg/m^3
μ_f	Viscosity of substrate solution, kg/m-s
$\varepsilon_f(z)$	Fractional liquid holdup in the fluidized bed at any z
μ_m	Maximum specific growth rate, s^{-1}
$\eta(z)$	Effectiveness factor at any cross-section z, dimensionless
$\eta_d(z)$	Parameter defined in equation (23), dimensionless
$\emptyset$	Thiele-type modulus, dimensionless
τ	Space time, s

I. Introduction

The objectives of the present study are two fold:

(i) To analyze the performance characteristics of a fluidized bed biofilm reactor of diverging-converging geometry and to compare its performance with that of a conventional fluidized bed bioreactor of cylindrical geometry but of same reactor volume.

(ii) To study the prospects of industrial production of polymer – grade lactic acid in the bioreactor of above proposed design, starting from economical raw materials such as molasses and cheese whey permeate.

Though diverging – converging geometries have displayed attractive augmentation features for the efficient design of heat and mass transfer equipment, this work is the first of its kind to investigate their adaptation to the design of fluidized bed bioreactors.

Mathematical simulation of hydrodynamics in constricted geometries has been attempted by many authors, though little work has been reported towards adaptation of these simulation results to industrial systems. Sparrow and Prata [1] have reported numerical solutions for laminar flow and heat transfer in a periodically converging-diverging tube, with experimental confirmation. Their study, however, is restricted to low Reynolds numbers (100 to 1000) and for Pr = 0.7, 2.5, 5.0. Mathematical solution of Navier-Stokes equation for unsteady (time – dependent) flow through periodically constricted tubes has been presented by Lahbabi and Chang [2]. Chandra and Prasad [3] have presented a mathematical study on the pulsatile flow in circular tubes of varying cross section. Nishimura and Matsune [4] have reported studies on pulsatile flow in asymmetric and symmetric channels with sinusoidal wavy walls at low Reynolds numbers. They observed that systems involving such pulsatile flow can be used to enhance heat and mass transfer in viscous liquids.

Heat transfer augmentation in sinusoidal wavy channels (based on experimental findings) has also been reported by Oyakawa, Shinzato and Mabuchi [5]. Kouris and Tsamopoulos [6] have reported mathematical simulation of annular flow of two immiscible fluids through tubes having sinusoidally varying cross section.

They observed that the viscosity ratio must remain strictly below unity and it has an optimum value which maximizes the range of allowed Reynolds numbers for stability. Newtonian flow through a two- dimensional wavy walled channel whose walls are lined with a thin poroelastic layer has been analyzed mathematically by Wei and coworkers [7]. Numerical investigation of unsteady flow and heat transfer in wavy channels has been reported also by Hossain and Islam [8]. They have solved two dimensional Navier-Stokes and energy equations numerically for unsteady laminar flow in periodic wavy(sinusoidal and triangular) channels.

Bahaidarah, Anand and Cher [9] have reported numerical studies on two – dimensional flow and heat transfer in periodic wavy channels as found in compact heat exchanger applications. Sinusoidal and arc –shaped channel configurations are considered in this study.

Dimakopoulos and Tsamopoulos [10] have reported studies on transient displacement of Newtonian liquids by gas in periodically constricted tubes.

They have examined the displacement of viscous liquids by pressurized gas from harmonically undulated tubes of finite length. An analytical study using perturbation methods has been reported by Thomas et al. [11] on the flow profiles and power requirements in an oscillating flow field with a wavy-walled boundary at low Reynolds numbers.

Akbari, Sinton and Bahrami [12] have studied laminar fully developed flow and pressure drop in linearly varying cross sectional converging diverging microtubes mathematically. They have developed an analytical model for frictional flow resistance assuming parabolic axial velocity profile. Ramgadia and Saha [13] have reported studies on fully developed flow and heat transfer characteristics in a wavy passage. They have used finite volume method on collocated grids to solve incompressible, time- dependent Navier-Stokes and energy equations in primitive variable form. Sochi [14] reports studies on Newtonian flow in converging - diverging capillaries. The one - dimensional Navier-Stokes equations are used to derive analytical expressions for the relation between pressure and volumetric flow rate in capillaries of five different converging diverging axisymmetric geometries for Newtonian fluids. The results are compared to the expressions derived by the author in his previous paper for the same geometries using the lubrication

Copyright © 2014 Praise Worthy Prize S.r.l. - All rights reserved

approximation.

Performance features of heat transfer and mass transfer equipment that employ tubes / flow channels of diverging – converging geometry have attracted a lot of research interest.

Design characteristics of variable area shell and tube heat exchangers (VAEs) have been discussed by Narayanan [15], [16] and it has been demonstrated that these exchangers operate with 250 – 300% increase in heat transfer coefficient, but with only 15 to 20% increase in the pressure drop penalty, as compared to the conventional shell and tube exchangers (that employ straight, cylindrical tubes) of same heat transfer area. The augmentation in heat transfer efficiency provided by these VAEs is thus truly phenomenal. The augmentation characteristics have been found to be of equal magnitude in the case of non – Newtonian flow (flow of suspensions and polymer solutions) through such geometries as well (Narayanan [17], [18]). Gas absorption in falling films on diverging – converging surfaces has also been studied by Narayanan [19], [20] and it has been found that falling film absorbers of such design provide 200 – 250% higher mass transfer coefficient (in liquid phase).

Condensation of pure vapors on diverging – converging tubes has been investigated both mathematically as well as experimentally by Chakraborty et al. [21] and in this case also, the rate of film condensation has been reported to be distinctly higher (as compared to straight tube condensers of same surface area per unit length). Experimental studies on mass transfer in an airlift fermenter of diverging – converging geometry have been reported by Ghosh, Maiti and Bhattacharya [22].

They have observed that both gas holdup and the liquid phase mass transfer coefficient are of higher magnitude when a diverging – converging riser is being employed.

Design of a constricted tube ultrafiltration unit with special reference to food processing (such as production of food grade protein concentrates from food wastes) has been described by Narayanan [23]. The proposed design of UF unit has been found to provide higher permeate flux, enhanced solute rejection and lesser problems of concentration polarization and membrane fouling as compared to traditional tubular UF modules of same membrane area per unit length. In the present study, attempts have been made to study the application of such diverging – converging geometries for the improved design of fluidized bed biofilm reactors.

II. Mathematical Modeling (Software Development)

The geometry of the bioreactor of proposed design is shown schematically in Fig. 1. The reactor column is of diverging-converging geometry having three segments.

Each segment has a diverging section and a converging section. By simple geometry, the angle of convergence / divergence (θ) is given as:

$$tan\,\theta = (D_2 - D_1) / L_S \quad (1)$$

where D_2 is the maximum diameter of the reactor column, D_1 is the minimum diameter and L_S is the length of each segment (see Fig. 1).

The dimensions of the column are chosen in such a way that $tan\,\theta$ = (1/12) and accordingly:

$$\theta \approx 5^0 \quad (2)$$

The diameter of the reactor column at any axial position z can be estimated as follows:

$$\text{For } z \le L_S/2 \qquad D(z) = D_1 + 2\,z\,tan\,\theta \quad (3)$$

$$\text{For } (L_S/2) \le z \le L_S, \qquad D(z) = D_1 + 2(L_S - z)\,tan\,\theta \quad (4)$$

$$\text{For } L_S \le z \le (3\,L_S/2) \qquad D(z) = 2\,[D_1 + (L_S + z)\,tan\,\theta] \quad (5)$$

$$\text{For } (3\,L_S/2) \le z \le 2\,L_S \qquad D(z) = 2\,[D_1 + 2\,(L_S - z)\,tan\,\theta] \quad (6)$$

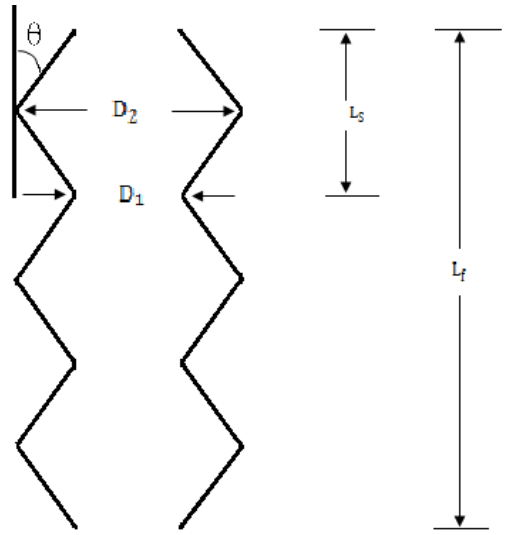

Fig. 1. Schematic of Reactor Column Geometry (Magnified View)

The reactor under consideration is a fluidized bed biofilm reactor. The feed solution (clarified molasses, cheese whey permeate) is admitted from the bottom where the column diameter = D_1 (minimum diameter) and it flows upward keeping the particle – biofilm aggregates in suspension. Each support particle (made of polymer composites, silica) is surrounded by a thin microbial solution of uniform thickness (δ) and these particle – biofilm aggregates remain suspended in the ascending stream of substrate solution. To simulate the performance of the bioreactor, it has been assumed to be equivalent to a Plug-Flow Dispersion Reactor (PFDR). Accordingly, the performance equation for the reactor shall be as given below:

Copyright © 2014 Praise Worthy Prize S.r.l. - All rights reserved

$$-U_{SUP}(z)[dC_S(z)/dz] + D_L[d^2C_S(z)/dz^2] = \eta(z)(-r_S)_{(int)} \quad (7)$$

where:

$$U_{SUP}(z) = 4\,Q_0 / [\pi \{D(z)\}^2] \quad (8)$$

D_L = axial dispersion coefficient, m^2/s, $\eta(z)$ = effectiveness factor.

To note that the superficial velocity of the substrate solution, U_{SUP}, varies along the height of the column due to the continuous change in the cross – sectional area of the column. The column diameter at any z, $D(z)$, has already been defined in Eqs. (3) to (6). The volumetric flow rate of the substrate solution is chosen in such a way that the superficial velocity of up-flowing solution lies above the minimum fluidization velocity, U_{mf}, at the inlet (corresponding to minimum cross section), but less than the terminal free settling velocity of the particle – biofilm aggregates (V_t). The minimum fluidization velocity (U_{mf}) at the inlet is estimated from the correlation proposed by Wen and Yu [24]which is given below:

$$Re_{mf} = [(33.67)^2 + 0.0408\,Ar_m]^{1/2} - 33.67 \quad (9)$$

Re_{mf} = Reynolds number at minimum fluidisation $= (d_{Pm} U_{mf}\,\rho_f)/\mu_f$ (10)

Ar_m = modified Archimedes number $= d_{Pm}^3\,(\rho_{Sm} - \rho_f)(g\,\rho_f/\mu_f^2)$ (11)

d_{Pm} = diameter of particle-biofilm aggregate, $m = (d_P + 2\delta)$ (12)

δ = biofilm thickness, m (assumed constant)

ρ_{Sm} = density of particle-biofilm aggregate, kg/m^3 $= f\,\rho_m + (1-f)\,\rho_S$ (13)

f = volume fraction of biofilm in aggregate $= 1 - (d_P/d_{Pm})^3$ (14)

ρ_m= density of microbial solution, kg/m^3

The terminal free settling velocity of particle – biofilm aggregates (V_t) is computed from the generalized settling law as:

$$V_t = [(4/3)(d_{Pm}) \cdot \cdot \{(\rho_{Sm} - \rho_f)/\rho_f\}(g/C_D)]^{0.5} \quad (15)$$

where C_D is the drag coefficient, the magnitude of which depends on the particle Reynolds number, Re_P:

$$Re_P = (d_{Pm} V_t\,\rho_f)/\mu_f \quad (16)$$

Eq. (15) is, therefore, solved by a trial and error procedure with the help of the standard C_D versus Re_P plot (Narayanan and Bhattacharya [25]). The biochemical processes considered are fermentation of molasses using *Enterococcus Faecalis* and that of cheese whey permeate (permeate obtained after separating whey proteins by ultrafiltration) using *Lactobacillus Helveticus* (both for the synthesis of polymer – grade lactic acid). Both of these reportedly follow Monod's kinetic equation.

Thus, the intrinsic rate of reaction is given by:

$$(-r_S)_{(int)} = \mu_m(app)\,C_S(z)/[K_S + C_S(z)] \quad (17)$$

where:

$$\mu_m(app) = (\mu_m\,x_f\,f/Y) \cdot \cdot [\{1 - \varepsilon_f(z)\}/\varepsilon_f(z)] \quad (18)$$

x_f = cell mass concentration in biofilm, gm/L (assumed constant).

For the fermentation of molasses (bioconversion of sucrose to lactic acid), the kinetic constants employed are those reported by by Anjana and Kumar [26] such as, μ_m =2.5641 hr^{-1}, K_S= 0.1 gm/L and Y= overall yield coefficient for cell mass production= 0.77. For the bioconversion of lactose (in cheese whey permeate) to lactic acid, Schepers and coworkers [27] report μ_m = 0.7 hr^{-1}, K_S = 0.22 gm/L and Y = 0.65. The fractional liquid holdup, $\varepsilon_f(z)$ is calculated from the correlation proposed by Richardson and Zaki [28] that has been observed to be quite reliable in the case of liquid-fluidized beds like the one under consideration. After substituting the expression for intrinsic rate from Eq. (17) in Eq. (7), it gets reduced to:

$$-U_{SUP}(z)[dC_S(z)/dz] + D_L[d^2C_S(z)/dz^2] = \eta(z)\,\mu_m(app)\,C_S(z)/[K_S + C_Z(z)] \quad (19)$$

The boundary conditions governing the system are:

B.C. 1: At z = 0

$C_S = C_{S0}$ = substrate concentration in feed solution (20)

B.C. 2 : At z = L_f ,

$C_S = C_{Se}$ = substrate concentration in product solution (21)

As stated earlier, the types of substrates considered are molasses and cheese whey. In the case of molasses, C_{S0} is the sucrose concentration and in the case of cheese whey permeate, C_{S0} is the lactose concentration. The axial dispersion coefficient (D_L) does change along the height of the reactor column. However, since the angle of divergence / convergence (θ) is only 5^0, this change has been observed to be not too substantial. Accordingly, an average experimental value of D_L that is based on tracer experiments (Narayanan [29]) has been used in the present analysis.

The effectiveness factor, η(z), is computed from the correlation proposed by Gottifredi and Gonzo [30], which is given below:

Copyright © 2014 Praise Worthy Prize S.r.l. - All rights reserved

$$[1/\eta(z)]^2 = \{1/\eta_d(z)\}^2 + \\ + \exp[\{6\,\emptyset^2 / \{5\,(1+\beta(z))^2\}\} + \\ - \{1/\eta_d(z)\}^2] \quad (22)$$

where:

$$\eta_d(z) = (\sqrt{2}/\emptyset)\,[\{1+\beta(z)\}/\beta(z)] \\ [\beta(z) - ln\,(1+\beta(z))]^{1/2} \quad (23)$$

$$\beta(z) = C_S(z)/K_S \quad (24)$$

$$\emptyset = L^*\,[\mu_m(app)/(K_S D_e)]^{1/2} \quad (25)$$

$$L^* = \text{characteristic length} = (V_P / S_P) = \\ [(\pi/6)\,d_{Pm}^3 - (\pi/6)\,d_P^3] / \pi\,d_{Pm}^2 \quad (26)$$

V_P, S_P=volume and surface area respectively of the biofilm,

D_e = effective diffusivity of substrate into the biofilm, m^2/s.

The above performance equation (Eq. (19)) is solved numerically based on the boundary conditions given in Eqs. (20) and (21) using a modified form of Fourth order Runge - Kutta Method.

Solution using line successive over – relaxation (SOR) method has also been attempted.

Both algorithms exhibited good stability and provided convergence within reasonable number of iterations.

The algorithms were executed at different values of feed flow rate, fractional substrate (sucrose/lactose) conversion attained and also at different values of biomass concentration in the biofilm.

The results obtained are presented and discussed in the subsequent sections.

To illustrate the specific advantages of the proposed design, the performance characteristics of the bioreactor of proposed design (of diverging - converging geometry) are compared with those of a bioreactor of conventional design (of straight, cylindrical geometry) but of same volume per unit length (in other words, of diameter D_V).

By definition therefore, D_V is the volumetric diameter of the bioreactor of proposed design and is nothing but the diameter of a straight cylindrical column of same volume per length as the diverging - converging column.

By simple geometry:

$$D_V = \sqrt{[(D_2^3 - D_1^3) / (3L_S\,tan\theta)]} \quad (27)$$

The developed software is therefore again executed by putting $D_2 = D_1 = D_V$ and the performance features of the bioreactor are estimated at different values of the substrate flow rate, substrate concentration and using the two sets of kinetic constants.

Computations are also performed at different values of biomass concentration in biofilm.

The same numerical algorithm has been employed in this case also. The results are illustrated in the next section.

III. Experimental Study (Materials and Methods)

Experiments were conducted on a laboratory bioreactor of following dimensions:

D_1 = minimum diameter = 1.0 m,

D_2 = maximum diameter = 1.1 m,

L_S = length of each segment = 1.0 m,

N = number of segments = 03.

Feed solutions employed: clarified molasses, cheese whey permeate. Raw cheese whey was first passed through an ultrafiltration unit to separate all the proteins as concentrate and the permeate, after diluting to 9.0 g/L (lactose concentration), is used as the substrate solution for the experiment. Sucrose concentration in feed molasses was 50 g/L. The support particles were 2.5 mm polymer composite beads and they were soaked in the microbial solution of *Enterococcus Faecalis* (when molasses was used as feed solution) and that of *Lactobacillus Helveticus* (when cheese whey permeate is used as substrate solution). The sucrose / lactose concentration in the exit solution from the reactor column is determined using a spectrophotometer and also with the help of a high performance liquid chromatograph (HPLC). Readings were recorded at different feed flow rates and at each flow rate, the experimental runs were repeated at least thrice so as to ascertain experimental consistency. Comparison between experimental data and those computed from the software package developed is illustrated in the next section.

IV. Results and Discussion

Comparison of experimental values of fractional conversion of substrate (α) attained with those computed mathematically from the developed simulation package is shown in Figs. 2 and 3. Fig. 2 is for fermentation of molasses and Fig. 3 considers lactic acid production from cheese whey permeate. It can be seen that the data predicted by the developed mathematical model agree closely with the experimental data compiled, the maximum deviation being ±10%. This thus ascertains the accuracy and reliability of the simulation package developed. It may be noted that from among the elaborate experimental data collected, a few selected data points are only shown in the figures (as illustrative examples). The software package is now re-executed at different values of process parameters to analyse the performance characteristics of the bioreactor of proposed design. The results are illustrated graphically in Figs. 4 to 8. Variation of fractional conversion of substrate attained (α) with substrate flow rate (Q_0) in the case of lactic acid production from molasses using *Enterococcus Faecalas* is illustrated in Fig. 4. The substrate concentration (sucrose concentration) in the feed solution (C_{S0}) is kept constant at 50.0 gm/L and the total height (L_f) of the fluidized bed (reaction zone) is fixed at 3.0 m. Data are illustrated for the case when biomass concentration in the biofilm (x_f) is 250 g/L and also when x_f is 275 g/L.

Copyright © 2014 Praise Worthy Prize S.r.l. - All rights reserved

Another set of plots illustrating variation of fractional conversion of substrate attained (α) with substrate flow rate (Q_0) in the case of lactic acid production from cheese whey permeate using *Lactobacillus Helveticus* are shown in Fig. 5. The substrate concentration (lactose concentration) in the feed solution (C_{S0}) is 9.0 gm/L and the total height (L_f) of the fluidized bed (reaction zone) 3.0 m. Data are illustrated for x_f = 150 gm/L and also when x_f = 175 gm/L.

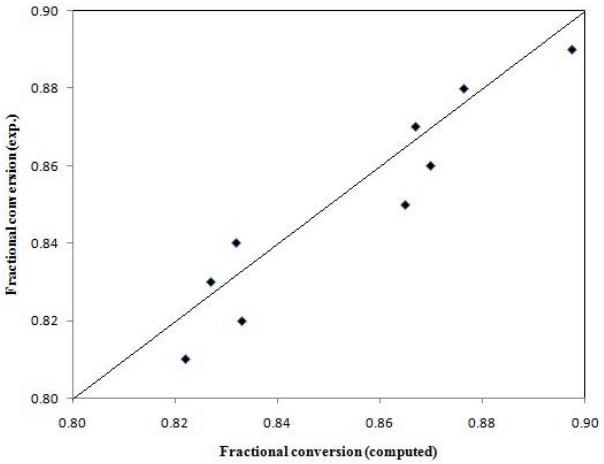

Fig. 2. Comparison between Experimental and Computed Values of Fractional Conversion of Substrate Attained (Molasses Fermentation)

Similarly, variation of fractional conversion of substrate attained (α) with substrate (sucrose / lactose) concentration in the fresh feed to the bioreactor (C_{S0}) is illustrated in Figs. 6 and 7. Figure 6 presents data on fermentation of molasses and Figure 7 those on lactic acid synthesis from cheese whey permeate. The biomass concentration in the biofilm (x_f) is 250 g/L for the former and 150 g/L for the latter. As shown in Fig. 4, when molasses is being used as feed solution, fractional conversion of substrate attained (α) decreases with increase in substrate flow rate (Q_0). This is understandable since an increase in substrate flowrate (Q_0) tends to decrease the average residence time of substrate in the reaction zone and consequently, the fractional conversion (α) attained decreases. On comparing the two plots of Fig. 4, it can be seen that the decrease of fractional conversion (α) with increase in substrate flow rate (Q_0) is much sharper when cell mass concentration in biofilm (x_f) = 250 gm / L. For example when substrate flow rate (Q_0) increases from 7 L/s to 9 L/s, fractional conversion (α) decreases from 0.86 to 0.836 (by 2.8 %), when cell mass concentration in biofilm (x_f) = 275 gm /L, while for the same increase in substrate flow rate (Q_0), the decrease in fractional conversion (α) is by 4.3% (from 0.84 to 0.804) when cell mass concentration in biofilm is 250 gm/L. It can also be observed that the fractional conversion (α) obtained at any specific flow rate is higher when x_f = 275 gm / L as compared to when x_f = 250 gm / L. This is understandable since increase in cell mass concentration in the biofilm (x_f) increases the intrinsic rate of bioconversion which, in turn, assists in providing larger fractional conversion (α) of substrate within the same reactor volume. Also, as stated earlier at, at low value of cell mass concentration in the biofilm (x_f = 250 gm/L), the fractional conversion (α) attained is more sensitive to change in substrate flow rate (reactor capacity).

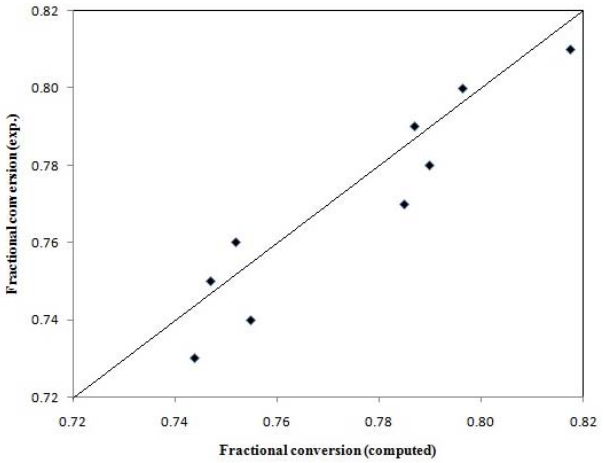

Fig. 3. Comparison between Experimental and Computed Values of Fractional Conversion of Substrate Attained (Fermentation of Cheese Whey Permeate)

The observation is similar when the cheese whey permeate is being used as the feed solution (Figure 5). It can be seen that the decrease in fractional conversion (α) is sharper at lower value of cell mass concentration in the biofilm (x_f = 150 gm/ L). For example, when the feed flow rate increases from 7 L/s to 9 L/s, the magnitude of fractional conversion (α) decreases from 0.81 to 0.77 (by 4.94 %) when cell mass concentration in the biofilm (x_f) = 175 gm / L, while the decrease in fractional conversion (α) is by 5.2 % (from 0.77 to 0.73) when cell mass concentration in the biofilm (x_f) = 150 gm / L. Further, as anticipated, the fractional conversion (α) of substrate (lactose) attained at any specific feed flow rate is higher when the cell mass concentration (x_f) in biofilm is higher.

Figs. 6 and 7 illustrate dependence of fractional conversion of substrate (α) attained on substrate (sucrose/ lactose) concentration in feed (C_{S0}) at specific values of feed flow rate (Q_0). It can be seen that the magnitude of fractional conversion (α) decreases with increase in substrate concentration in the feed (C_{S0}) at any specific value of substrate flow rate (Q_0). The observation is identical with all values of biomass concentration in biofilm (x_f) and also with different kinetic constants (with both feed solutions such as molasses and cheese whey permeate).

At a given value of C_{S0} (sucrose/ lactose concentration in feed), the reactor provides higher fractional conversion when the feed flow rate is lower.

Since the expanded bed height of the bioreactor (L_f) is kept constant at 3.0 m, a lower feed flow rate shall provide larger residence time (τ) of substrate in the reaction zone and thus helps in achieving larger fractional conversion (α).

Copyright © 2014 Praise Worthy Prize S.r.l. - All rights reserved

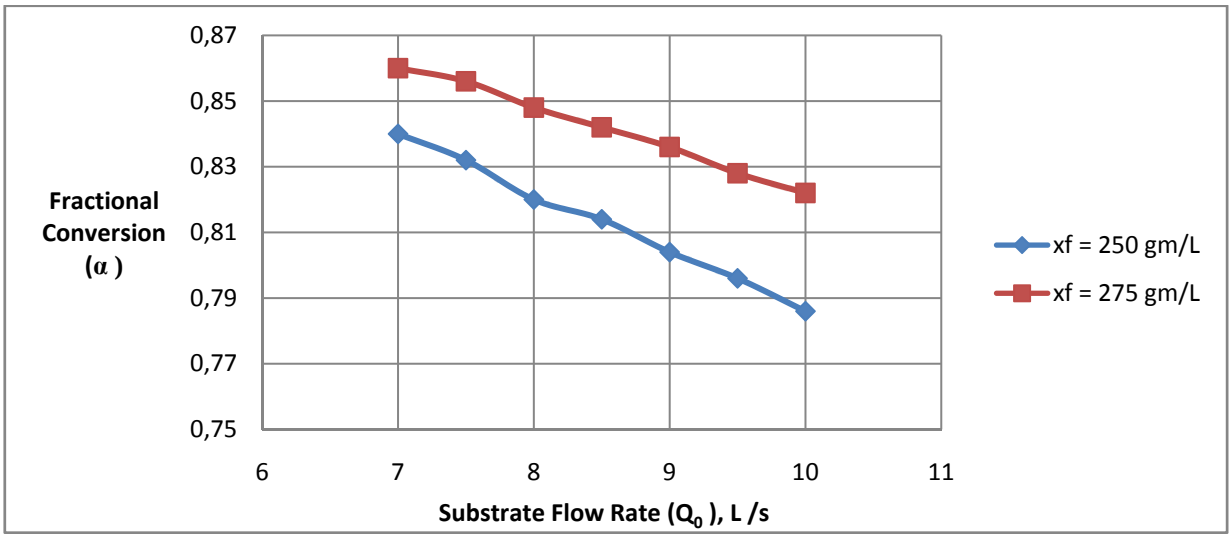

Fig. 4. Variation of Fractional Conversion of Substrate Attained (α) with Substrate Flowrate (Q_0) for Molasses Fermentation. Cell Mass Concentration in Biofilm (x_f) = 250 gm/L (upper curve), 275 gm/L (lower curve)

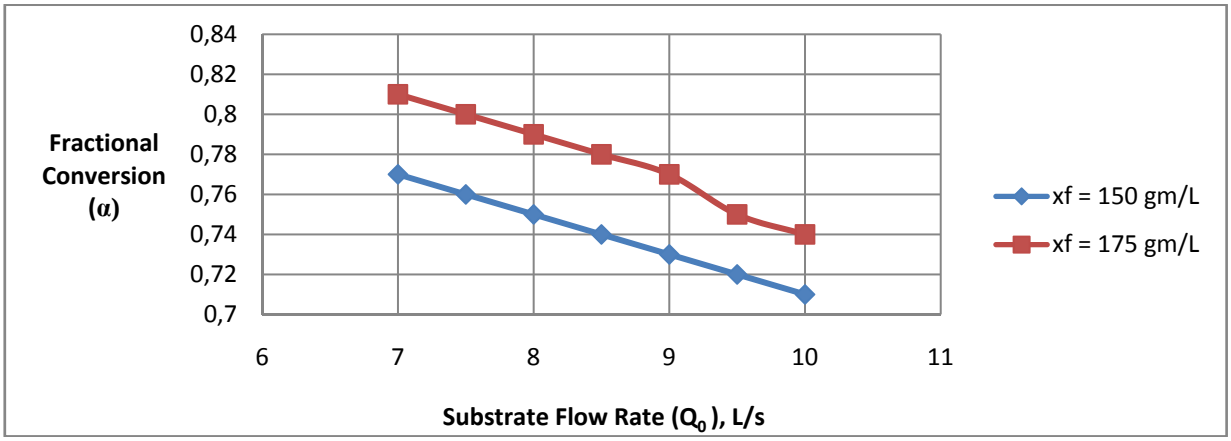

Fig. 5. Variation of Fractional Conversion of Substrate Attained (α) with Substrate Flowrate (Q_0) for Cheese Whey Fermentation. Cell Mass Concentration in Biofilm (x_f) = 150 gm/L (upper curve), 175 gm/L (lower curve)

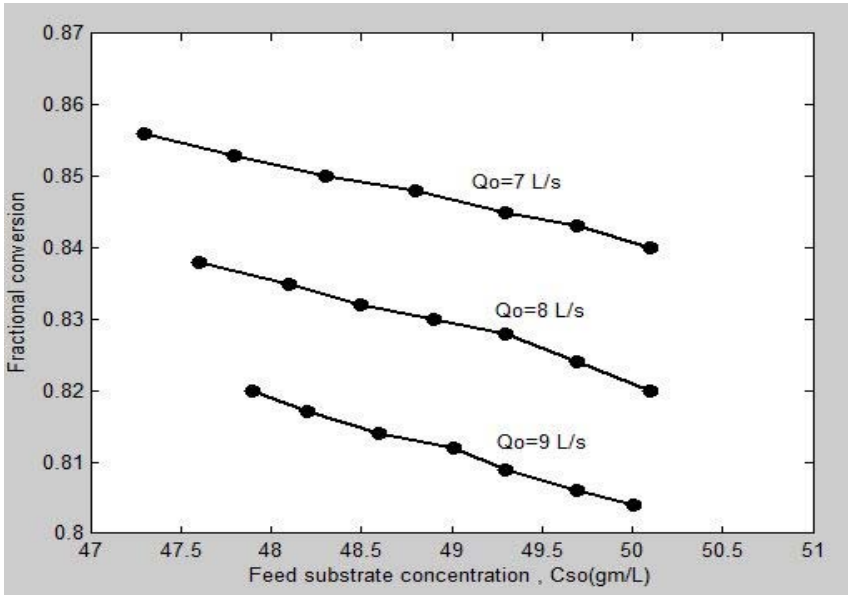

Fig. 6. Variation of Fractional Conversion of Substrate Attained (α) with Initial Substrate (sucrose) Concentration (C_{s0}) at Different Values of Substrate Flowrate (Q_0). Cell Mass Concentration in Biofilm (x_f) = 250 gm/L

Copyright © 2014 Praise Worthy Prize S.r.l. - All rights reserved

The above figures (graphical illustrations) thus help in making an optimum choice of process parameters such as substrate flow rate (Q_0) to be employed and cell mass concentration to be maintained in the biofilm (x_f) to attain a given fractional conversion (α) of substrate, while handling a feed solution of substrate concentration = C_{S0} in a bioreactor of expanded bed height, L_f .

Comparison between performance characteristics of the bioreactor of proposed design and those of a conventional fluidized bed bioreactor (of uniform cylindrical geometry) of same volume per unit length (that is, of diameter D_V) is shown in Figures 8 and 9.

The former considers lactic acid production from molasses and the latter cheese whey permeate fermentation. A typical set of plots illustrating the variation of percentage enhancement in fractional conversion with substrate flowrate (Q_0) is shown in Fig. 10. In this figure, curves – 1 and 3 correspond to cheese whey fermentation, while curves – 2 and 4 correspond to molasses fermentation.

It can be seen that the bioreactor of proposed design provides significantly higher fractional conversion (α) of substrate at any specific value of feed flow rate (Q_0) as compared to the bioreactor of straight, cylindrical geometry. This observation is identical in the case of both feed stocks handled (molasses as well as cheese whey permeate), both types of kinetic equations and at all values of biomass concentration in biofilm (x_f).

The percentage enhancement in fractional conversion (α) ranges from 21.0 % to 29.0 %, within a feed flowrate (Q_0) ranging from 7 L/s to 10 L/s, substrate concentration (C_{S0}) in feed solution ranging from 45.0 to 50.0 gm / L (for sucrose) and 5.5 to 9.0 gm / L for (lactose).

The bioreactor of proposed design thus provides augmented performance efficiency at the same operating conditions. The percentage enhancement increases with increase in feed flow rate (Q_0) at lower values of cell mass concentration (x_f) in biofilm (such as 150.0 gm / L, 250 gm/L) as shown in Fig. 10. However, at large values of cell mass concentration in biofilm (x_f = 175.0 gm /L, 275 gm/L), the percentage enhancement exhibits a slightly decreasing trend with increase in feed flow rate (Q_0).

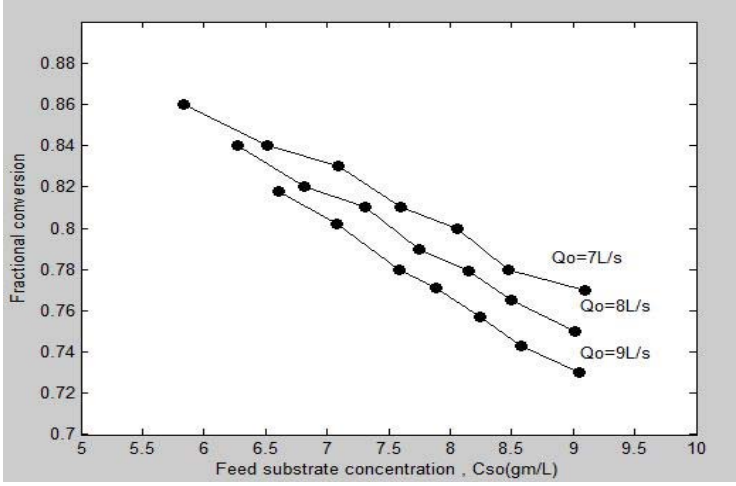

Fig. 7. Variation of Fractional Conversion of Substrate Attained (α) With Initial Substrate (lactose) Concentration (C_{S0})), Cell Mass Concentration in Biofilm (x_f) = 150 gm/L

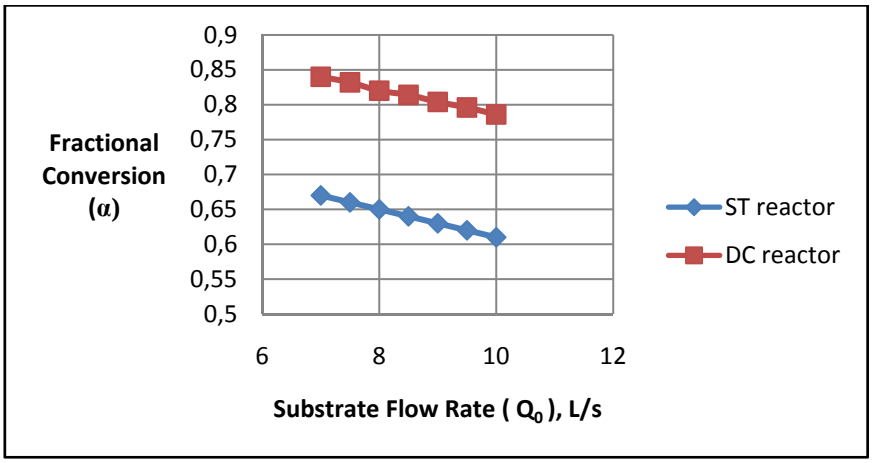

Fig. 8. Comparison Between Performance of Bioreactor of Proposed Design and that of Bioreactor of Conventional Design (of Same Reactor Volume), for Molasses Fermentation. Cell Mass Concentration in Biofilm (x_f) = 250 gm/L

Copyright © 2014 Praise Worthy Prize S.r.l. - All rights reserved

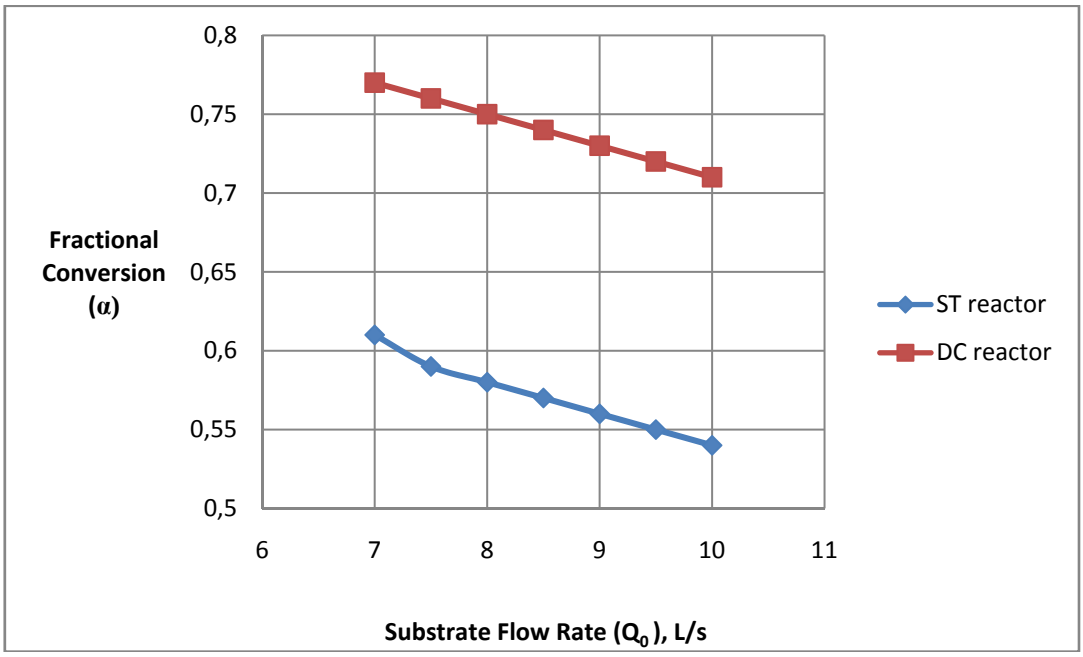

Fig. 9. Comparison Between Performance of Bioreactor of Proposed Design and that of Bioreactor of Conventional Design (of Same Reactor Volume), for Cheese Whey Permeate Fermentation. Cell Mass Concentration in Biofilm (x_f) = 150 gm/L

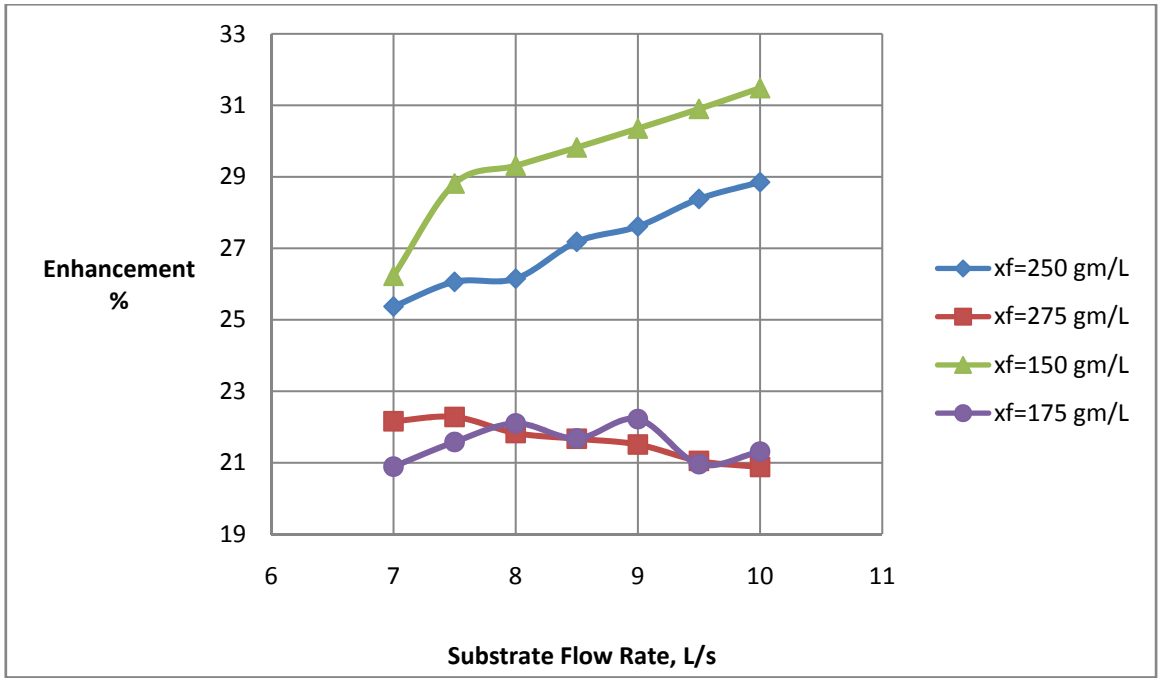

Fig. 10. Variation of Percentage Enhancement in fractional conversion attained with Substrate Flow rate

A similar trend has been observed regarding the variation of percentage enhancement with increase in substrate concentration (C_{S0}) in the feed solution. At larger values of of cell mass concentration (x_f) in biofilm (x_f = 175.0 gm/L, 275 gm/L), the percentage enhancement sluggishly increases with increase in substrate concentration (C_{S0}), but at lower value of cell mass concentration (x_f) in biofilm (x_f = 150.0 g/L) the percentage enhancement exhibits a decreasing trend with increase in substrate concentration. The decrease, however, is not substantial.

V. Conclusion

1. The performance characteristics of a fluidized bed biofilm reactor of diverging – converging geometry have been analyzed mathematically and a versatile software package has been developed. The reliability of the package has been duly verified by comparing with elaborate experimental data collected. The maximum deviation between computed values of process variables and the experimental data compiled has been found to be ± 10%.

Copyright © 2014 Praise Worthy Prize S.r.l. - All rights reserved

2. The bioreactor of proposed geometry is found to provide enhanced fractional conversion of substrate (20 to 30% higher) as compared to a conventional fluidized bed reactor of same volume per unit length. This is true with both types of feedstocks (molasses and cheese whey permeate), both sets of kinetic parameters and at all values of cell mass concentration in the biofilm. The percentage enhancement increases with increase in substrate flow rate at low values of $x_{f,}$ but shows a sluggishly decreasing trend at high values of biomass concentration (x_f).
3. The improved performance exhibited by the diverging – converging fluidized bed bioreactor may be attributed to several factors:
   a) The minimum fluidization velocity (U_{mf}) is selected based on cross section – 1 (inlet cross section, corresponding to minimum diameter D_1). At this cross section, the bed is fully fluidized which helps in speedy start-up of the reaction. As the partially converted feed solution moves up, the cross-sectional area of the reactor increases, thereby increasing the residence time (τ). At cross section – 2 (corresponding to maximum diameter D_2), the fluid elements receive maximum residence time. This helps in achieving larger fractional conversion (α) of the substrate. As the product solution (with a small percentage of unconverted substrate) moves further up, the cross- sectional area decreases, the turbulence increases. There shall be more intimate mixing among fluid elements and this facilitates further bioconversion, even though the substrate concentration is at a lower level.
   b) If the fractional conversion (α) attained is not high enough, then the reaction mixture enters the second diverging section, where due to gradual increase in reactor volume, additional (and higher) residence time is provided to attain higher conversion. This is followed by the second converging section where, as stated earlier, more efficient contacting between fluid elements occurs to bring the bioconversion to the ultimate desired level.
   c) Experimentally, it has been estimated that the value of axial dispersion coefficient (D_L) is lower for a diverging – converging tube as compared to a straight, cylindrical tube of same volume per unit length [Narayanan, 2011]. Typically, the experimental value of axial dispersion coefficient (D_L) for a diverging – converging column is 0.02 m^2/s while that for a straight, cylindrical column of diameter D_V is 0.0315 m^2/s. Radial dispersion is of high magnitude in a diverging – converging tube and this provided an uniform concentration of substrate at any particular cross-section inside the reactor (with little radial variation). However, due to the lower degree of axial dispersion, the system dynamics tends to approach plug flow and this tends to improve the reactor performance.
4. The prospects of industrial adaptation of the bioreactor of proposed design must be, therefore, anticipated to be quite bright.

Acknowledgements

The authors is thankful to his young students, Ms. Ananya Basak, Arpita Saha and Soni Jha and to all of the fellow members of IRG (International Research Group), consultancy firms and software companies of India and Europe for their cooperation during the execution of this project.

This paper has been presented and discussed in the Chemical Engineering Congress held at Mumbai, India during December 27 – 30, 2013 and has been subsequently modified based on the suggestions and recommendations received during the conference.

References

[1] Sparrow, E.M. and Prata, A.T., Numerical Solutions For Laminar Flow And Heat Transfer in a Periodically Converging-Diverging Tube with Experimental Confirmation, *Numerical Heat Transfer*, Volume 6, No.4, pp.441 – 461, 1983.

[2] Lahbabi, A. and Chang, H.C., Flow In Periodically Constricted Tubes: Transition to Inertial State, *Chemical Engineering Science*, Volume 41, No. 10, pp.2487-2505, 1986.

[3] Chandra, P. and Prasad, J.S.V.R.K., Pulsatile Flow In Circular Tubes Of Varying Cross-Section With Suction / Injection, *J. Austral. Math. Soc*., Ser. B 35, pp.366-381, 1994.

[4] Nishimura, T. and Matsune, S., Vortices And Wall Shear Stresses In Asymmetric And Symmetric Channels With Sinusoidal Wavy Walls For Pulsatile Flow At Low Reynolds Numbers, *Int. J. Heat and Fluid Flow*, Volume 19, No. 6, pp.583-593, 1998.

[5] Oyakawa, K, Shinzato, T and Mabuchi, I., The Effects Of The Channel Width On Heat Transfer Augmentation In A Sinusoidal Wave Channel, *JSME International Journal*, Series II, Volume 32, No. 3, 403 – 410 1998.

[6] Kouris, C. and Tsamopoulos, J., Core Annular Flow in a Periodically Constrictetd Tube - Part I : Steady State, Linear Stability And Energy Analysis, *J. Fluid Mech.*, Volume 432, Issue 01, pp.31 – 68, 2001.

[7] Wei, H.H., Waters, S.L., Liu, S.Q. and Grotberg, J.B., Flow In A Wavy – Walled Channel Lined With a Poroelastic Layer, *J. Fluid Mech*.,Volume 492, pp. 23-45,2003.

[8] Hossain, M. Z. and Islam, A.K.M.S., Numerical Investigation Of Unsteady Flow And Heat Transfer In Wavy Channels, *Proc. Australian Fluid Mechanics Conference*, Sydney, December 13-17, 2004.

[9] Bahaidarah, H.M.S., Anand, N.K., Numerical Study Of Heat And Momentum Transfer In Channels With Wavy Walls, *Numerical Heat Transfer*, Part A, Volume 47, 417-439, 2005.

[10] Dimakopoulos, Y. and Tsamopoulos, J., Transient Displacement Of Newtonian Liquids By Gas In Periodically Constricted Tubes, *AlChE Journal*, Volume 52, Issue 8, pp.2707-2726, 2006.

[11] Thomas, A.M., Thich, G.K. and Narayanan, R., Low Reynolds Number Flow In A Channel With Oscillating Wavy Walls - An Analytical Study, *Chemical Engineering Science*, Volume 61, No. 18, pp.6047-6056, 2006.

[12] Akbari, M, Sinton, D. and Bahrami, M., Laminar Fully Developed Flow In Periodically Converging-Diverging Microtubes, *Heat Transfer Engineering* , Volume 31, No. 8, pp. 628-634, 2010.

[13] Ramgadia, A.G.and Saha, A.K., Fully Developed Flow And Heat Transfer Characteristics In A Wavy Passage: Effect Of Amplitude Of Waviness And Reynolds Number, *International J. Heat and Mass Transfer*, Volume 55, No. 9-10, pp.2494-2509, 2012.

Copyright © 2014 Praise Worthy Prize S.r.l. - All rights reserved

[14] Sochi, T., Newtonian Flow In Converging Diverging Capillaries, arXiv: 1108.0163v1[math – ph], pp.1 – 20, 2012.
[15] Narayanan, C.M. and Bhattacharya ,B.C., Studies on Heat Transfer in Diverging Converging Geometries, *Industrial and Engineering Chemistry Research*, Volume 27, No.1, pp. 149 – 155, 1988.
[16] Narayanan, C.M., Studies on Performance Characteristics of Variable Area Heat Exchangers, *J. Chemical Engineering Japan*, Volume 31, No.6, pp.903 – 909, 1998.
[17] Narayanan, C.M. et.al, Studies on Non – Newtonian Flow and Heat Transfer in Wavy tubes, *Mech. Engg. Bull*, Volume 25, No.3 &4, pp.69 – 75, 1994.
[18] Narayanan, C.M., Studies on Transport Phenomena in Polymer Solutions and Suspensions flowing through Tubes of Tortuous Wall Geometry, *Heat and Mass Transfer (Wärme und Stoffübertragung)*, Vol.50, Issue 2, 161 – 168, 2014.
[19] Narayanan C.M., Transport Phenomena in Falling films on Diverging – Converging Surfaces, *Ind. J. Technology*, Volume 25, No.4, pp.176 – 84, 1987.
[20] Narayanan, C.M., Studies on Gas Absorption with Chemical Reaction in Falling films on Wavy Surfaces, *J. Energy Heat Mass Transfer*, Volume 15, pp.305 – 310, 1993.
[21] Chakravarty, T.K., Narayanan, C.M. and Bhattacharya, B.C., Experimental Studies On Heat Transfer With Phase Change On Diverging-Converging Surfaces, The *Canadian Journal of Chemical Engineering*, Volume 69, No. 1, pp.281-285, 2009.
[22] Ghosh , T.K., Maiti , B.R. and Bhattacharya, B.C., Gas Hold Up In Converging Diverging Tube Airlift Fermenter, *Biotechnology Techniques*, Volume 7, No. 4, pp.301-307, 1993.
[23] Narayanan, C.M., Performance Analysis of Constricted Tube Ultrafiltration Unit for the Production of Food Grade Protein Concentrates from Food Wastes, *Journal of Chemical Engineering and Materials Science*, Volume 2, No. 9, pp. 149-155, 2011.
[24] Wen, C. Y. and Yu, Y. H., A Generalized Method For Predicting The Minimum Fluidization Velocity, *AIChE J*, Volume 12, No. 3, pp.610-612, 1966.
[25] Narayanan, C.M. and Bhattacharya, B.C., Mechanical Operations for Chemical Engineers, Khanna Publishers, New Delhi, 1992.
[26] Anjana, D.N. and Kumar, S., Kinetic Modeling Of Lactic Acid Production From Molasses using *Enterococcus Faecalis RKY1*, *Biochemical engineering Journal*, Volume 38, pp.77-84, 2008.
[27] Schepers, A.W. et.al, Continuous Lactic Acid Production In Whey Permeate/Yeast Extract Medium With Immobilised *Lactobacillus Helveticus*, *Enzyme Microb.Technology*, Volume 30, pp.176-186, 2002; Volume 38, pp.24-37, 2008.
[28] Richardson, J.F. and Zaki, W.N., Sedimentation and Fluidization - Part I., *Trans. Inst. Chem. Eng*, Volume 32, pp.35-53, 1954.
[29] Narayanan, C. M., Process Analysis, Simulation and Software Development – A Few Applications (*Invited Lecture*), *Proc. International Conference on Recent Advances in Chemical Engineering*, Cochin, March 10 – 12, 2011.
[30] Gottifredi, J.C. and Gonzo, E.E., Approximate Expression For Effectiveness Factor Estimation, *Chemical Eng. J.*, Volume 109, pp.83-87, 2005.

Authors' information

Department of Chemical Engineering,
National Institute of Technology, Durgapur,
India.
E-mail: cmn_recd@yahoo.co.in
Website: www.profcmn.com

Copyright © 2014 Praise Worthy Prize S.r.l. - All rights reserved

Praise Worthy Prize

International Review of Chemical Engineering (I.RE.CH.E.), Vol. 6, N. 4
ISSN 2035-1755 *July 2014*

Kinetic and Isotherm Studies of Adsorption of Lead (II) Ion Onto Functionalized Nigeria Ahoko Kaolin

Kovo A. S., Olu S. C., E. A. Afolabi

Abstract – *The kinetic and thermodynamic of lead (II) adsorption onto functionalized and unfunctionalized Nigeria Ahoko kaolin was studied with the aim to investigate the sorption potential of kaolinite clay as a commercial adsorbent in removal of Pb2+ from aqueous solution. The effect of various variables namely initial concentration of Pb2+, contact time and temperature were investigated. The equilibrium data were obtained using batch experiment process only. The equilibrium data was fitted to the three isotherm model used namely: Freundlich, Langmuir and Temkin, with Temkin having the best fit than the other with coefficient of determination R2 approximately one, while the pseudo-second order best explained the kinetics of the adsorption process. Increasing initial Pb2+ concentration, increased the rate of Pb2+ adsorbed and the initial rate of sorption h for both adsorbent, also increase in temperature from 298 K to 323 K was also observed to increase the initial sorption rate h from 10.07 to 139.07 (mg/g.min) and 9.43 to 78.57 (mg/g.min) for functionalized and unfunctionalized respectively. The adsorption reaction for both adsorbent was found to be a chemically activated reaction and endothermic with activation energy E for the 1000(mg/L) of Pb2+ in solution as 1089.78 and 3424.73 (KJ/mol) for functionalized and unfunctionalized adsorbent respectively. The positive values of the enthalpy and the entropy change suggests that the endothermic nature of the adsorption and the negative values of free energy change indicate the feasibility and spontaneity nature of the adsorption process.* ***Copyright © 2014 Praise Worthy Prize S.r.l. - All rights reserved.***

Keywords*: Kaolin, Kinetic, Adsorption, Lead (II), Thermodynamic, Isotherm, Functionalized*

I. Introduction

Due to rapid industrialization, there have be indiscriminate and excessive release of heavy metals into the ecosystem, thus creating a serious and significant concerns worldwide, this is because of the negative and adverse effects of heavy metals on humans, and animal's health and the ecosystem in general [1]-[18].

Industrial wastewater often contain heavy metals such as chromium, nickel, arsenic, platinum, cadmium, palladium, zinc, copper, mercury, and lead which occur as a result of industrial activities ranging from plating of metals, geological activities, blacksmithing, manufacturing of batteries, refining of petroleum and petrochemicals, manufacturing of paints and pigments, insecticides and pesticides manufacturing etc.

The removal of deleterious metals such as lead from the ecosystem is becoming an important study because of the awareness of increasing pollution of the environment by heavy metals. Lead serves as raw materials in the industry for manufacturing of lead storage batteries, photographic materials, pigments, leaded glass, fuel, pencils, matches and explosives for the usage of man [11]. It is also one of the deleterious metals, usually present in waste streams from geological and mining operations, electronics, electroplating, petroleum and petrochemical industries [17].

It is a pollutant that is present in water bodies, soil and in air. In air, it serves as an anti-knocking agent in gasoline (the form of lead tetraethyl) which results to lead emission from automobiles, while in water; it is release as effluent especially in lead batteries manufacturing units, lead treatment and recovery industries.

The toxicity of lead to living organism is very pronounce in that when release into the environment can both accumulate and enter the food chain, hence causing serious malfunctioning in humans such as mental retardation, decreases production of haemoglobin essential in the transport of oxygen and cellular metabolic abnormality [18]. The damaging effect of lead is conspicuous mostly on the nervous system of the body, which result in the reduction in the I.Q's level in children. Lead. WHO, 1971 reported 0.10mg/l as the highest permissible limit of lead that is allowed in drinking water and FEPA, 1991 also report that the maximum lead concentration discharge allowed for inland water should be less than 1mg/l [6].

Electrolysis, flocculation and sedimentation, Solvent extraction, distillation, ion exchange, reverse osmosis, wet oxidation, and adsorption are among the several methods been suggested for wastewater treatment especially those poisoned and polluted with heavy deleterious metals [4].

Copyright © 2014 Praise Worthy Prize S.r.l. - All rights reserved

Adsorption onto activated carbon having a better adsorptive capacity for wide range of various forms and types of adsorbates, which have been discovered to be much more efficient and effective relative to the above mentioned methods [1], but Chakraborty [2], pointed out the disadvantage of the usage of activated carbon as having a very high cost price.

Because of the cost of the activated carbon, several research have taken place to study other cheaper alternative substituent, that are less expensive, having the same time endowment and a similar capacity for adsorption as activated carbon.

II. Materials and Method

The materials used in this research study are kaolinite clay, chemicals such as tripolyphosphate (VI) solution, hydrogen peroxide, sodium hydroxide, distilled and deionised water.

II.1. Kaolin Collection and Pre-Treatment

The kaolin used in this research work was gotten from Ahoko, Kogi State, Nigeria. After collection, some solid, metallic and other hefty materials were eliminated from the kaolin sample. The sample was also sieved using a 250 µm Sieve in order to eliminate particles which are not clay from the kaolin sample and 500 g of the kaolin sample was suspended into distilled water in a 1000ml beaker for 8.0 hours.

Moore and Reynolds method was used to purify the raw kaolin sample; this method involves the treatment of the sample with small quantity of thirty percent hydrogen peroxide solution until all effervescence stopped.

The Moore and Reynolds method of treatment of the kaolinite clay was performed in order to remove any organic particles left in the clay. The treated sample was left for 24.0 hours and then there was decantation of the supernatant, and deionised water was used to thoroughly wash the kaolin sample left, in order to eliminate any remnant of hydrogen peroxide left in the kaolinite clay sample.

The sludge suspended kaolin was dried using an electric oven at a temperature of 363K to obtain a dried kaolin clay sample used.

II.2. Functionalization/Modification of the Kaolin

100g of the kaolin clay sample were brought into an equilibrium state with 2 litres of 200 mg/L of Sodium Tripolyphosphate($Na_5P_3O_{10}$) using a magnetic stirrer at a revolution of 250rpm for 5.0 hours and centrifuged at 2000rpm for 10.0 minutes, to ensure thorough equilibration. The kaolin samples were then washed thoroughly with 1000 mL of distilled water to remove excess $P_3O_{10}^-$ ions, until the phosphate test is found to be negative.

The electric oven was then used to dry the functionalized kaolin clay at a temperature of 363 K.

II.3. Kinetics of Lead (II) Ion Adsorption

1.0 g/litre each of stock solution of a standard lead (II) was made from Lead (II) nitrate ($Pb(NO_3)_2$) with distilled water. The solutions with lead (II) ion of concentration of 250, 500, and 1000 mg/L were prepared and the pH adjusted to 6.0±0.2 with 0.10 mol/litre sodium hydroxide. Kinetic experimental studies were performed on a batch adsorption method at a temperature of 25^{o}C on a water bath shaker at 250 rpm using 120 mL polyethylene bottles comprising of 100 mL of 250, 500 and 1000 mg/litre of initial concentration lead (II) solutions and 5.0 g of the functionalized and unfunctionalized kaolin samples. 10.0 mL of the aliquots/suspensions were drawn out from the 100 mL of the lead (II) solution in the water bath shaker at distinct time interval. The withdrawn suspensions were then centrifuged at 4000 rpm for 10.0 minutes and the supernatants were analyzed using Atomic Absorption Spectrometer for the quantity of lead (II) ions.

The above procedure was repeated at temperatures of 298, 308, and 323 K using 1.0 g/L concentration of the stock lead (II) ion solution with the functionalized and unfunctionalized kaolin samples, to study the effect of temperature on the kinetic of lead (II) ion sorption process. Blank samples without the kaolinite clay samples used in this research work were also analyzed.

The amount of Pb^{2+} adsorbed by the kaolinite clay sample was evaluated using:

$$q_e = \frac{(C_o - C_e)V}{W(g)} \quad (1)$$

where:

q_e concentration of metal ion adsorbed by the kaolin sample at equilibrium (mg/L).

Co denotes the initial metal ion concentration (mg/L).

C_e denotes the equilibrium concentration of the metal ion (mg/L).

V denotes the volume of adsorbate (L).

W denotes the weight of the adsorbents used (g).

The experimental readings were obtained using an Atomic Absorption Spectrometer (AAS). The air-acetylene flame was used and absorption lines used is 283.3 nm.

III. Results and Discussion

III.1. Characterization of Starting Material (NAK)

The XRD pattern of the refined NAK sample (Fig. 1) shows a sharp and narrow peak with a basal reflection at $2\theta = 12.37^o$ (d= 7.15 Å). The peak position of refined NAK is comparable to that of raw NAK sample.

The surface morphology of both the refined and coarse raw NAK samples were studied by SEM to also verify and authenticate that the refinement of NAK has actually taken place. The SEM image of the refined NAK (Fig. 2) lucidly show kaolinite particles with irregular and erratic sizes.

Copyright © 2014 Praise Worthy Prize S.r.l. - All rights reserved

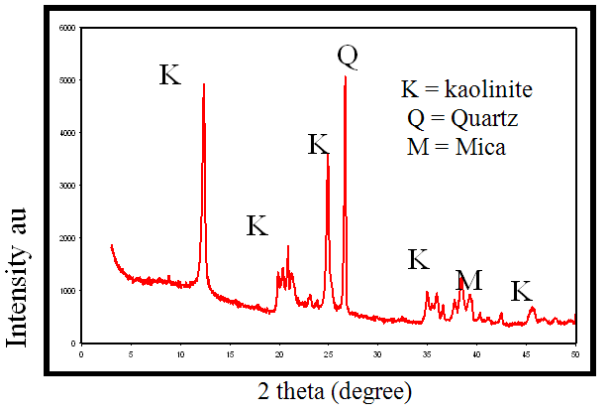

Fig. 1. XRD pattern of functionalized Nigeria Ahoko Kaolin

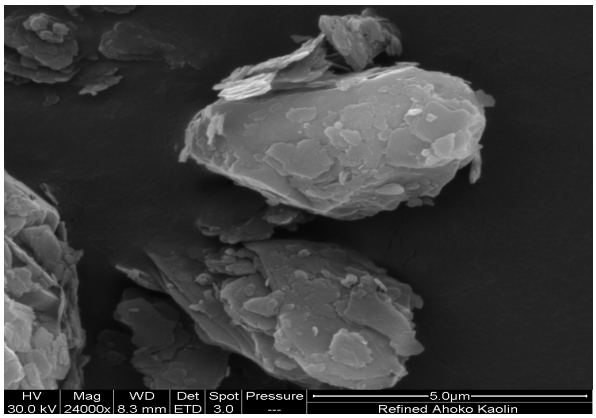

Fig. 2. The SEM image of functionalized Nigeria Ahoko Kaolin

This is as a result of a low crystal-width to thickness ratio ([3], [9]).

Both the usual pseudo-hexagonal platelet and the rough edge were similarly noticed in majority of the particles, conversely the observed platelets reveals thinness of kaolinite flakes suggesting finesse/refinement nature of the kaolin surface [8], [7] and [10].

III.2. Kinetics Study

III.2.1. Effects of Initial Lead Concentration on Kinetics of Lead (II) Ion Adsorption

Figs. 3 and 4 present the adsorption capacity of both functionalized and unfunctionalized kaolin as a function of lead (II) ion initial concentration and time. The figures show the amount of Pb^{2+} adsorbed q_t(mg/g) and the adsorbed quantity of lead (II) ion per unit time increases with contact time between the adsorbate and adsorbent at all initial lead (II) ion concentration ([13], [15]), also from Figs. 1 and 2, the slope obtained was used to evaluate the rate of sorption.

The rates of adsorption of lead (II) ion on both the functionalized and unfunctionalized kaolin sample in the first 10 minutes were observed to increase from 0.479 to 1.915 and 0.340 to 1.894 ($mgg^{-1}min^{-1}$) for both functionalized and unfunctionalized kaolin sample respectively with an increase in the initial lead (II) ion concentration from 250 to 1000 mg/L respectively. At time interval of 10 to 70 minutes, the adsorption rate of lead (II) ion decreases to 0.071, 0.120, 0.281 and 0.0675, 0.140, 0.274 ($mgg^{-1}min^{-1}$) for the functionalized and unfunctionalized kaolin sample respectively of 250, 500, and 1000 (mg/L) initial lead (II) concentration respectively.

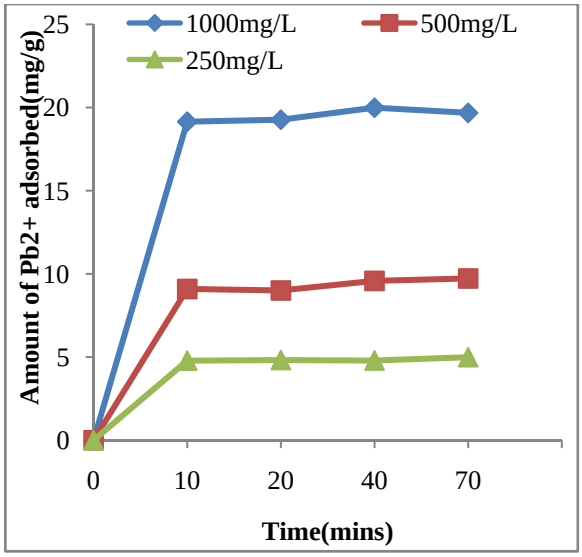

Fig. 3. Effect of varying concentration of Pb^{2+} on functionalized kaolinite clay at various contact time

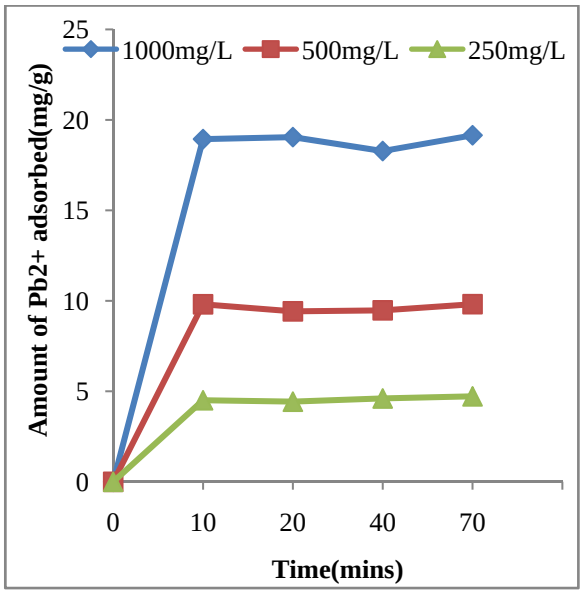

Fig. 4. Effect of varying concentration of Pb^{2+} on unfunctionalized kaolinite clay at various contact time

The initial steep adsorption curve in Figs. 3 and 4 suggests a rapid adsorption on the surface of both functionalized and the unfunctionalized adsorbent for the first 10 minutes and later became slower till an equilibrium is attained. The large initial adsorption rate is owing to the increased in the number of empty adsorption spot existing in the early phase of the adsorption processes.

Copyright © 2014 Praise Worthy Prize S.r.l. - All rights reserved

The equilibrium data obtained were evaluated using the pseudo first–order and pseudo second-order models.

The pseudo-first-order model show a very poor fit after the first 10.0 minutes of reaction with time but the pseudo-second-order produce a very appropriate fit for all reaction time as shown in Figs. 5 and 6 for the functionalized and unfunctionalized respectively. Figs. 5 and 6 present a linear relationship between the t/q_t and time for the functionalized and unfunctionalized kaolin adsorbent at distinct concentration of lead (II) ion. The initial adsorption rate h, pseudo-second-order rate constant k_2 and the quantity of lead (II) ion adsorbed at equilibrium q_e were found using the pseudo-second-order model as shown in Table I.

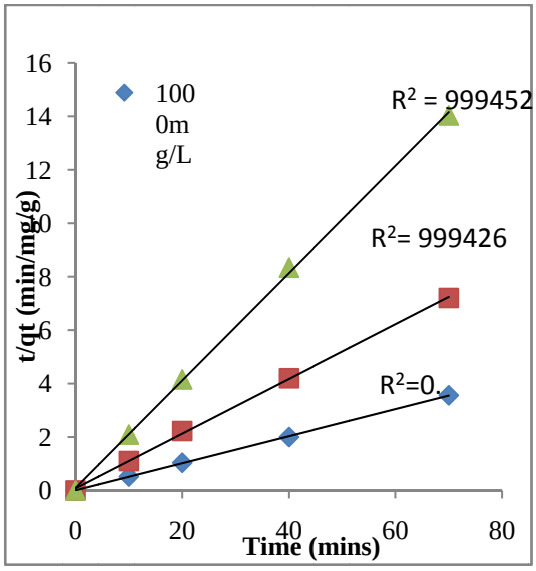

Fig. 5. Pseudo-second order plots for adsorption of Pb ions on functionalized sorbent at 298 K

Increasing the concentration of lead (II) ion also increases the initial sorption rate, from 10.07 to 139.07 and 9.434 to 78.57 ($mgg^{-1}min^{-1}$)for functionalized and unfunctionalized kaolin sample respectively as the concentration of lead (II) ion increases from 250 to 1000 (mg/L). The quantity of the adsorbed lead (II) ion at equilibrium q_e was evaluated from the slope of Figs. 3 and 4, and the values obtained followed same trend showing an increase from 4.981 to 19.765 and 4.727 to 19.029 (mgg^{-1}) for functionalized and unfunctionalized kaolin sample respectively of 250 to 1000 (mg/L) initial lead (II) ion concentration respectively, but a decrease in the pseudo-second-order constant K_2 as presented in Table I.

Modification/Functionalization of kaolin increases the initial sorption rate, specifically at a very high concentration. The linear format of the second-order model of the kinetics in Figs. 5 and 6 suggests a chemical adsorption reaction rather than a physical adsorption reaction ([15], [16]). The equivalent linear charts of k, h, and q_e of the adsorption process are often presented as a function of C_o for the Pb^{2+} adsorption using functionalized and unfunctionalized kaolin samples.

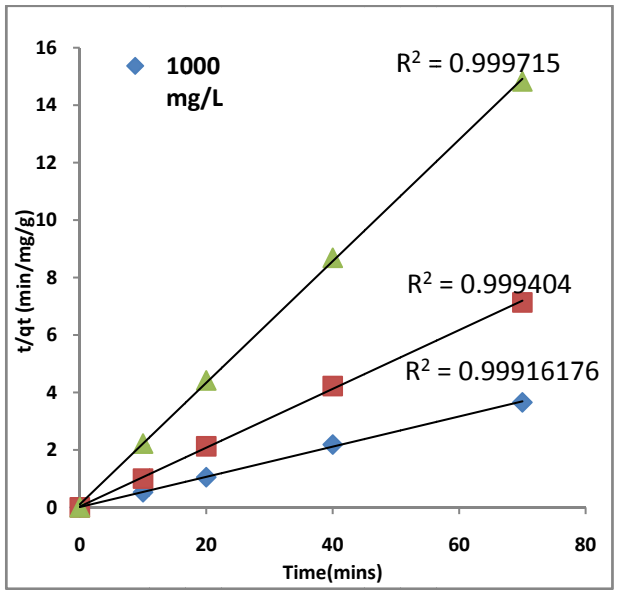

Fig. 6. Pseudo-second order plots for adsorption of Pb^{2+} ions on functionalized sorbent at 298 K

For the Functionalized kaolin, the following correlation are obtained:

$$q_e = 0.019752C_o - 0.01557 \quad R^2 = 0.999895$$
$$K = 0.4185 - 6.42857E\text{-}05C_o \quad R^2 = 0.9642857$$
$$h = 0.176766C_o - 41.27 \quad R^2 = 0.980752$$

For unfunctionalized kaolin, the following correlation are obtained:

$$q_e = 0.01899C_o - 0.098155 \quad R^2 = 0.999531$$
$$K = 0.4825 - 0.00027C_o \quad R^2 = 0.992572$$
$$h = 0.092244C_o - 13.721 \quad R^2 = 0.999987539$$

The validity of the order of sorption processes is based on two basic criteria, namely regression coefficient and calculated q_e, [15] as obtained from the regression correlation coefficients and slopes of Figs. 5 and 6 respectively. However the coefficient of relationship of the sorption process R^2 and the quantity of lead (II) ion adsorbed at equilibrium q_e for pseudo-second order model have very high values as presented in Table I.

III.2.2. The Effects of Temperature on Kinetics Lead (II) Ion Adsorption

The plot of the linearize type of the second order model for 1000 (mg/L) concentration of Pb^{2+} adsorption at varying temperatures. Differences in temperature influences the time needed to attain equilibrium in the sorption of Pb^{2+}.

Table I shows that increase in temperature also increases both pseudo-second-order rate constant K_2 and the initial sorption rate h, on the functionalized and unfunctionalized kaolin samples. The data obtained for the pseudo-second-order rate constant K_2 showed an increase from 0.365 to 0.426 ($mgg^{-1}min^{-1}$) and 0.217 to

Copyright © 2014 Praise Worthy Prize S.r.l. - All rights reserved

0.296 ($mgg^{-1}min^{-1}$) with temperature increase from 298 to 323 K for functionalized and unfunctionalized adsorbent respectively. This indicating that increase in temperature will also cause an increase of the energetic force of lead (II) ion [5].

Also the correlation existing between pseudo-second-order rate constant K_2 and temperature is used in determining the activation energy and this is described with equation as shown below:

$$K_2 = K_o exp\left(\frac{-E}{RT}\right) \quad (2)$$

K_2 denotes rate constant of adsorption of pseudo-second-order ($mgg^{-1}min^{-1}$),
K_o denotes temperature-independent coefficient ($mgg^{-1}min^{-1}$),
E denotes adsorption activation energy ($KJmol^{-1}$),
R is the gas constant (8.314 $Jmol^{-1}K^{-1}$),
T denotes absolute Temperature (K).

Fig. 7 presents a graph of lnK against 1/T, which produced a rectilinear with $\frac{-E}{RT}$ as the slope of the graph.

The size of the activation energy provides an insight on the adsorption type, which can either physical or chemical. In physical the activation energy is often small, and it is a reversible reaction while in chemical, the activation energy is high.

The values of the activation energy E obtained are 9993.43 and 5075.714 $KJmol^{-1}$ for functionalized and unfunctionalized samples respectively for 1000 (mg/L) concentration of lead (II) ion.

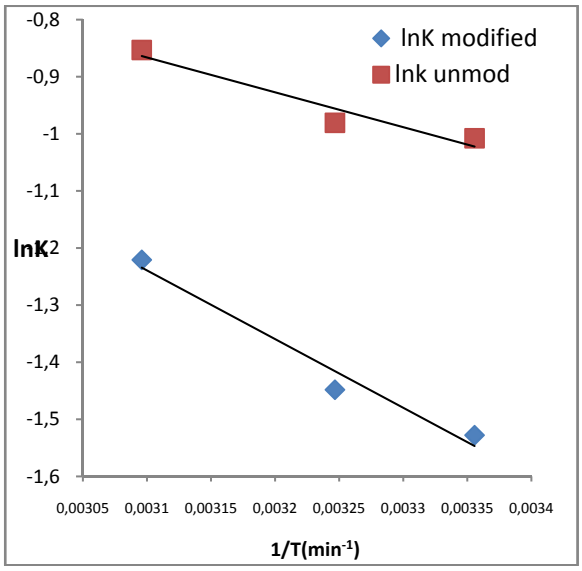

Fig. 7. Relationship between T and K for functionalized and unfunctionalized clay (Pb^{2+} =1000(mg/L))

III.3. Intraparticle Diffusion

The intraparticle diffusion model proposed by Weber and Moris provided the rate of intraparticle diffusion by a relationship between q_t and root of time $t^{1/2}$ as:

$$q_t = k_{id} t^{\frac{1}{2}} + C_i \quad (3)$$

The intraparticle diffusion rate was evaluated with the aid of plot q_t versus $T^{0.5}$ (see Figs. 8 and 9) for both functionalized and unfunctionalized kaolin.

Where k_{id} is the intraparticle diffusion rate constant and C_i is the association to the boundary layer thickness [13].

III.4. Adsorption Isotherm

Adsorption isotherms are arithmetical models that describes the dispersion of the adsorbate types between the liquid and solid, based on some postulations which are associated to the degree of uniformity of the solid surface, the types of handling and analysis as well as the probability of interaction among the adsorbate species.

In this work, the study of the lead (II) ion sorption is limited to the Freundlich, Langmuir and the Temkin isotherm model.

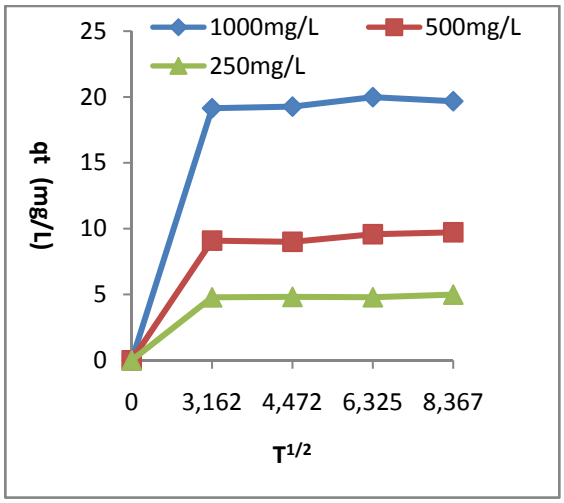

Fig. 8. Intraparticle diffusion plot for adsorption of Pb^{2+} onto functionalized kaolinite clay

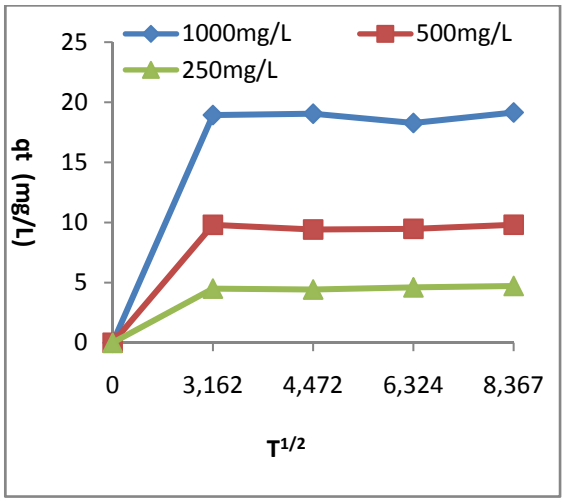

Fig. 9. Intraparticle diffusion plot for adsorption of Pb^{2+} onto unfunctionalized kaolinite clay

Copyright © 2014 Praise Worthy Prize S.r.l. - All rights reserved

III.4.1. Freundlich Isotherm Model

The equilibrium data from Pb^{2+} sorption on both functionalized and unfunctionalized Nigeria Ahoko Kaolin were fitted to the Freundlich model equation.

The results obtained from the adsorption of the Pb^{2+} in the batch study using three initial concentrations on both kaolinite clay samples were plotted logarithmically. The Freundlich parameters were obtained from the Freundlich Eq. (4) via the logarithmic plot and are shown in Table II:

$$log\ q = log\ K + \frac{1}{n} log\ C \quad (4)$$

III.4.2. Langmuir Isotherm Model

The estimation of the highest sorption rate is often evaluated using Langmuir model to determine it equivalent to the degree of monolayer coverage onto both kaolin samples. The plot of Langmuir isotherm not shown was used determining parameters q_m, K_L and its coefficient of determination R^2 for 1000, 500, and 250 (mg/L) respectively.

The values of the isotherm's parameters and R^2 were obtained as intercept, slope and regression correlation from the plots and are presented as shown in Table II.

The coefficient of determination R^2 shows that the Langmuir model have a better fitting than the Freundlich model.

III.4.3. Temkin Isotherm Model

The Temkin adsorption isotherm model for the three initial concentration (i.e. 1000, 500, and 250 (mg/L)) and the isotherms parameters are given in Table II. The intercept and slope of the plots are used in evaluating the Temkin constants K_T and B_T respectively.

The coefficient of determination R^2 of the Temkin model especially for modified kaolin give values approximately 1.0 for initial concentration of the lead (II) ion, showing the Temkin gives a better isotherm fitting than the Freundlich and Langmuir isotherm model.

TABLE I
FITTING OF KINETICS PARAMETERS OF ADSORPTION ACCORDING TO PSEUDO-SECOND ORDER RATE AT VARYING INITIAL CONCENTRATION OF Pb^{2+} IONS ONTO FUNCTIONALIZED AND UNFUNCTIONALIZED ADSORBENT AT 298 K AND INTRAPARTICLE DIFFUSION

Adsorbent	Kinetic Parameter				Intraparticle Diffusion model		
Functionalized Initial Conc	q_e(mg/g)	K_2 (g/mg/min	h (mg/g/min)	R^2	K_{id} (mg/gh$^{0.5}$)	C_i	R^2
C_o (1000 mg/L)	19.765	0.356	139.07	0.9998	2.211	5.745	0.646
C_o (500 mg/L)	9.773	0.381	36.39	0.9994	1.090	2.609	0.682
C_o (250 mg/L)	4.9808	0.406	10.07	0.9995	0.550	1.420	0.649
Unfunctionalized							
C_o (1000 mg/L)	19.029	0.217	78.57	0.9992	2.088	5.762	0.617
C_o (500 mg/L)	9.771	0.338	32.26	0.9994	1.071	2.920	0.623
C_o (250 mg/L)	4.727	0.422	9.434	0.9997	0.525	1.310	0664

TABLE II
ISOTHERM PARAMETER FOR PB (II) ADSORPTION ONTO FUNCTIONALIZED AND UNFUNCTIONALIZED KAOLIN

Adsorbent	**ISOTHERMS**								
	Langmuir			**Freundlich**			**Temkim**		
	q_m (mg/g)	K_L (L/g)	R^2	1/n	K_f (L/g)	R^2	K_T (L/g)	B_T (KJ/mol)	R^2
Functionalized Kaolin									
C_o(1000mg/L)	19.074	-4.322	1.000	-0.012	20.142	0.875	0.139	19.552	1.00
C_o(500 mg/L)	8.519	-0.467	0.994	-0.051	11.241	0.280	0.292	9.351	1.00
C_o (250 mg/L)	1.176	0.083	0.912	-0.018	5.010	0.992	0.557	4.880	1.00
Unfunctionalized kaolin									
C_o(1000mg/L)	17.451	-0.253	1.000	-0.067	24.704	0.994	5.797e-9	-1.260	0.994
C_o(500 mg/L)	9.772	10.244	0.995	0.021	9.218	0.164	4.070	0.204	0.164
C_o (250 mg/L)	4.243	-0.816	0.998	-0.118	0.882	6.493	5.719	-0.403	0.990

IV. Conclusion

The experimental results from the research study were analyzed using the Freundlich, Langmuir and the Temkin isotherm model. After evaluation of the data obtained using the isotherm models, the regression correlation coefficient/ coefficient of determination R^2 from the isotherm models showed that Temkin isotherm model describe the data more appropriable than the Freundlich and Langmuir isotherm model, especially with functionalized kaolin sample. The adsorption process follows a pseudo second-order kinetics, where the functionalization/modification of kaolin with tripolyphosphate (VI) increases the performance of Pb^{2+} adsorption rate onto the kaolin. There is an increase in both the amount Pb^{2+} adsorbed and initial sorption rates but a decrease in the overall Pb^{2+} sorption rate onto both kaolinite clay samples (i.e. functionalized and unfunctionalized) with an increasing concentration of lead (II) ion in the aqueous solution.

It is expedient to also note that temperature affects the adsorption processes, as increase in temperature
results to increase in the initial sorption rate as well as increase in the amount of lead (II) ion adsorbed from

Copyright © 2014 Praise Worthy Prize S.r.l. - All rights reserved

aqueous solution by the functionalized and unfunctionalized kaolin samples.

References

[1] Ahmad, A.A., Hameed, B.H. and Aziz, N. Adsorption of direct dye on palm ash: kinetic and equilibrium modelling. *Journal of Hazardous Materials*, Vol. *094*, (2006), *1-10.*

[2] Chakraborty, S., De, S., DasGupta, S., and Basu, J.K. Adsorption study for the removal of basic dye: *experimental and modelling. Chemosphere*, Vol. 58, (2005), 1079-1089.

[3] Frost, R.L., Marek Zbik, V.D.G., Kloprogge, J.T., and Paroz, G.N. Birdwood kaolinite: a highly ordered kaolinite that is difficult to intercalate an XRD, SEM and Raman spectroscopy study. *Applied Clay Science*, Vol. 20: (2002), 177-187.

[4] Gupta, V.K. and Sharma, S. Removal of Zinc from Aqueous SolutionsUsing Bagasse Fly Ash - a Low Cost Adsorbent. *Industrial and Engineering Chemistry Research Vol. 42,* (2003), *6619–6624.*

[5] Hefne, J.A., Mekhemer, W.K., Alandis, N.M., Aldayel, O.A. and Alajyan, T. Kinetic and thermodynamic study of the adsorption of Pb (II) from aqueous solution to the natural and treated bentonite. *International Journal of Physical Sciences, Vol.* 3(11), (2008), 281-288.

[6] Joel, T. N. Low Blood Lead Level Associated with Clinically Diagnosed Attention-Deficit/Hyperactivity Disorder and Mediated by Weak Cognitive Control, Society of Biological Psychiatry *63, 325-326 (2008).*

[7] Kovo, A. S. Kaolin to zeolite conversion, kaolin refinement, zeolites synthesis and identification. *LAP LAMBERT academic publishing, 480-510, (2011).*

[8] Lori, J.A., Lawal, A.O., and Ekanem, E.J. Characterization and optimization of deferration of Kankara clay.*ARPN Journal of Engineering & Applied Science,* Vol. 4, (2007), 60-73.

[9] Nakagawa, M., M.S., S. Yoshikura, M. Miura, T. Fukuda, A. Harada, *Kaolin deposit at Melthonnakkal and Pallipuram within Trivandrum block southern India* Gondwana Research, Vol. 9, (2006), 530-538.

[10] Ramaswamy, S.C.S. Investigation of a grey kaolin from south east India *Applied Clay Science,* Vol 3, (2007), 32-46.

[11] Raji, C. and Anirudhan, T.S. Chromium (IV) adsorption by sawdust carbon: Kinetics and equilibrium. *Indian Journal of Chemical Technology*, Vol. 4(5), (1997), 228-236.

[12] Rushdi, I. Y., Bassam, E., and Ala'a, H. A. Adsorption characteristic of natural zeolites as solid adsorbents for phenol removal from aqueous solution: Kinetics, mechanism, and thermodynamics studies. *Chemical Engineering Journal, Vol.* 171 (2011), 1143-1149.

[13] Teoh, Y. P., Khan, A. M., and Choong T. S. Kinetic and isotherm studies for lead adsorption from aqueous phase on carbon monolith. *Chemical engineering journal* Vol. 217, (2013), 248-255.

[14] Xiao-ming, L., Zheng, W., Wang, D., Yang, Q., Cao, J., Yue, X., Shen, T. and Zeng, G. Removal of Pb (II) from aqueous solutions by adsorption onto modified areca waste: Kinetic and thermodynamic studies. *Desalination Vol.* 258, (2010), 148–153.

[15] Unuabonah, E.I., Olu-Owolabi, B.I., Adebowale, K.O. and Ofomaja, A.E. Adsorption of lead and cadmium ions from aqueous solutions by tripolyphosphate-impregnated kaolinite clay. *Colloids Surfaces A: PhysicochemEng Aspects* Vol. 292: (2007), 202–211.

[16] Vasuderan P, Padmavathy, V. and Dhingra, S.C. (2003). Kinetics of biosorption of cadmium on Baker's yeast. *Bioresour. Technol*. Vol. 89(3), (2003), 281–287.

[17] Qaiser, S., Saleem, A.R. and Ahmed, M.M. Heavy metal uptake by agro based waste materials. *Environmental Biotechnol.* 10(3), (2007), 1-8.

[18] Williams, C. J. Comparison between biosorption for the removal of metal ion from aqueous solution. *Water Res*. Vol. 32. (1998),215-225.

Authors' information

Department of Chemical Engineering,
Federal University of Technology,
Minna.
E-mail: kovoabdulsalami@gmail.com

Copyright © 2014 Praise Worthy Prize S.r.l. - All rights reserved

Praise Worthy Prize

International Review of Chemical Engineering (I.RE.CH.E.), Vol. 6, N. 4
ISSN 2035-1755 *July 2014*

Pyrolysed Carbon-Silica Filler Obtained by Pyrolysis-Cum-Water Vapour of Waste Green Tires *vs.* Conventional Fillers. Comparison of Their Effects Upon the Properties of Epoxidized Natural Rubber Based Vulcanizates

Omar A. Al-Hartomy[1], Ahmed A. Al-Ghamdi[1], Said A. Farha Al Said[1], Nikolay Dishovsky[2], Mihail Mihaylov[2], Milcho Ivanov[2], Petar Kolev[2], Ljutzkan Ljutzkanov[3]

Abstract – *Pyrolysed carbon-silica filler (PCSF) has been obtained via pyrolysis cum water vapour of waste "green" tire treads. Weight analyses as well as AAS and ICP-OES analyses show that PCSF consists of 60% of silica, 36% of carbon black, 2.5% of zinc oxide and of about 1.5% of different oxides. As FTIR spectra and TEM micrographs show, the selected pyrolysis conditions allow silica and carbon black used as fillers in tires manufacturing to preserve their particle size and surface chemical activity in the pyrolysed product. The vulcanization characteristics, mechanical and dynamic properties of composites based on epoxidized natural rubber reinforced with the pyrolysed carbon-silica filler (PCSF) have been studied in comparison to those of analogous composites comprising conventional fillers. It has been established that the vulcanization characteristics, mechanical and dynamic properties of the studied rubber compounds and vulcanizates filled with PCSF are commensurable, even in some cases improved, in comparison to those of the composites comprising the conventional fillers.* ***Copyright © 2014 Praise Worthy Prize S.r.l. - All rights reserved.***

Keywords*: Waste Green Tires, Pyrolysis, Silica, Rubber Composites, Mechanical Properties*

I. Introduction

Within the past few decades, the technical tire community has suggested many innovative solutions to contribute to improvements in automotive fuel efficiency.

Tire companies have provided new products (from novel tire constructions to new material systems) in response to the increasing demands for higher mileage gasoline vehicles. The technical community has done research on the opportunities for improving tires rolling resistance while maintaining the critical balance of the other facets of the "magic triangle" - all season traction and wear [1].

One specific area of researchers' focus has been the usage of new raw materials for tire tread. Tread formulations have a large impact on key tire performance attributes such as rolling resistance, traction and wear.

Typically, either styrene butadiene rubber (SBR) or blends of SBR with polybutadiene or natural rubber are compounded with processing oils, fillers, cross-linking agents and additives.

Fillers are used in tread formulations to reinforce the elastomers and improve wear resistance, but these materials also contribute to energy dissipation in the compound.

During the 1990s, widespread replacement of carbon black filler with silica filler was pioneered by a major tire manufacturer as the "green tire concept".

Using silica filler with silane coupling agents provided unique properties such that rolling resistance was lowered and wet grip improved without detriment to tread life [1].

In the recent years the company Cabot Corporation has developed new types of functionalized carbon black to improve the tradeoff between wear resistance and rolling resistance. Those include chemically modified carbon black with different functional groups and carbon-metal oxide-multiphase composites produced by the co-fuming process.

The company has also presented a dual phase filler of the carbon-silica type (CSDPF 2000) as a market product ECOBLACK^{TM}CRX^{TM}2XXX. With this material, the filler-filler interaction is substantially reduced due to the surface modification. The polymer-filler interaction is enhanced by increasing the surface energy of the carbon domain of the filler and by the formation of chemical bonds via a coupling reaction between polymer chains and silanols on the silica domain. As a result the rolling resistance is lowered and wet grip improved [2]. All said above reveals the crucial role that the type of both elastomer and filler has in improving the tires exploitation properties.

Nowadays there has been a worldwide tendency for replacing the synthetic petrol products with such of renewable sources viewing environment protection.

Copyright © 2014 Praise Worthy Prize S.r.l. - All rights reserved

In accordance with the said tendency, in 2006 Dunlop launched to the market a new type of environmentally friendly tires under the branch name, ENASAVE ES801". Only 30% of the ingredients in those tires are petrol derivatives. The tires comprise epoxidized natural rubber (ENR) and silica in the tread. Mineral oil has been replaced by vegetable oil and synthetic fiber by vegetable fiber [3]. Hence, the new eco-tires are minimum dependent on petrol sources. It is known that the surface of silica particles is hydrophilic – it has silanol and hydroxyl groups what leads to aggregation of silica particles. Therefore they are not dispersed evenly in the rubber matrix during the compounding. Besides, the vulcanization agents (sulphur and vulcanization accelerators) are also adsorbed on silica surface. So, the vulcanization time is prolonged which results into a poorer reinforcement effect of the filler. A better dispersion of silica and a stronger polymer-filler interaction are achieved using different types of silane coupling agents [4]. Being of polar character, ENR is reinforced via silica better even in the absence of organosilanes. Therefore the tire treads based on ENR/silica are of lower rolling resistance and better wet road grip, if compared to those based on NR/silica or SBR/silica [3].

The utilization of great number of tires results into immense amounts of waste. According to statistics, annually the waste tires in the European Union countries amount about 2 500 000 tons, as much as those in North America and about 1 000 000 tons in Japan [5]. That waste is a valuable source of energy and materials. On the other hand, waste tires being resistant to moisture, oxygen, ozone, microbiological factors, etc. are of great environmental concern. The waste tires pyrolysis could be an environmentally friendly solution as its products have a significant potential for wide range of applications. The process turns the waste tires into pyrolytic oil, pyrolytic gas and pyrolytic solid residue (carbon black). The derived oils may be used directly as fuel or added to petroleum refinery feedstock.

The gaseous products are also useful as fuel, and the carbon black may be used as reinforcing filler in rubber or as activated carbon because of its high carbon content [6]. Under the conventional conditions the pyrolysis of vulcanizates comprising silica having silanol groups over its surface could lead to undesired calcification parted by agglomeration of silica particles. The pyrolysis-cum-water vapour of silica filled vulcanizates run according to the method of L. Ljutzkanov [7] is supposed to preserve the silanol groups in the pyrolysis product as well as to restore those that have reacted with the silane coupling additives. The product thus obtained could find application in rubber industry and be tantamount to widely used conventional silica [8], [9].

This paper presents the characterization of the solid product yielded from pyrolysis-cum-water vapour of waste green tires tread (Michelin Energy 195/65 R 15) as well as its filler effect upon the properties of composites based on epoxidized natural rubber (Epoxyprene 25).

II. Experimental Methods

II.1. Materials

The investigations were performed using the following materials:

Epoxidized natural rubber – Epoxyprene 25, containing 25±2% epoxy groups, distributed randomly in the polymer chain. Epoxyprene 25 was purchased from San -Thap International Co., Ltd. Its characteristics were: glass transition temperature (Tg) - 47ºC; density 0.97 g/cm^3; Mooney viscosity ML(1+4)100ºC ~ 80-100 MU.

Carbon black Corax N220 was purchased from Orion Engineered Carbons. Its characteristics were: average diameter of the particles ~20-40 nm; iodine adsorption 121 mg/g; statistical thickness surface area (STSA) 106 m^2/g; oil absorption number (OAN) 114 ml/100g and pour density 350 g/dm^3.

Silica, Ultrasil 7000 GR from Evonik Industries had the following characteristics: specific surface area (N_2) 175 m^2/g; specific surface area (CTAB) 160 m^2/g; loss on drying 5.2%; pour density 270 g/l; electrical conductivity ≤ 1300 μS/cm.

The pyrolysed carbon-silica filler (PCSF) was obtained via pyrolysis-cum-water vapour of waste green tires tread (Michelin Energy 195/65 R15) by L. Ljutzkanov [7] at the Institute of Chemical Engineering, Bulgarian Academy of Sciences.

The other ingredients such as zinc oxide (ZnO), Stearic acid (SA), bis (triethoxysilylpropyl) tetrasulfide (TESPT, Si 69), N-tert-butyl-2-benzothiazolesulfenamide (TBBS) and sulphur were also of commercial grades.

II.2. Measurements

The ash content of the pyrolysed carbon-silica filler (PCSF) was determined according to ISO 1125:1999.

The ash from the pyrolysed carbon-silica filler (PCSF) was studied by silicate analyses, weight analysis, atomic absorption spectroscopy – AAS (Perkin Elmer 5000), inductively coupled plasma-optical emission spectroscopy - ICP-OES ("Prodigy" High Dispersion ICP-OES, Teledyne Lemas Labs) and infrared spectroscopy with Fourier transformation (VARIAN 660-FTIR Spectrometer, KBr pellet). The particles size, size distribution and some specific features of the pyrolysed carbon-silica filler were determined using a TEM JEOL 2100 at an accelerating voltage of 200 kV.

The specimens were prepared by grinding the samples in an agate mortar and dispersing them in ethanol by ultrasonic treatment for 6 min. A droplet of the suspension was dripped on standard carbon films on Cu grids. The vulcanization characteristics of the rubber composites were determined at 150ºC on a Moving Die Rheometer (MDR 2000 Alpha Technologies) according to ISO 3417:2008. The mechanical properties of the composites studied were determined according to ISO 37:2011. Shore A hardness of the composites studied were determined according to ISO 7619-1:2010, while the wear resistance - according to ISO 4649:2010.

Copyright © 2014 Praise Worthy Prize S.r.l. - All rights reserved

The complex dynamic modulus and the heat build-up were determined on a Goodrich flexometer at a 850 min^{-1} deformation rate. Dynamic properties (Dynamic storage modulus (E') and mechanical loss angle tangent (tan δ)) of the studied composites were investigated using a Dynamic Mechanical Thermal Analyzer Mk III system (Rheometric Scientific).

The data were obtained at a frequency of 5 Hz and strain amplitude of 64 μm in the temperature range from -80ºC to 80ºC using a heating rate of 3ºC/min under single cantilever bending mode. The dimensions of the investigated samples were as follows - width 10 mm, length 25 mm and the thickness measured using a micrometer varied between 1 and 2 mm.

II.3. Preparation of Rubber Composites

The formulations of the compounds based on epoxidized natural rubber – Epoxyprene 25 are presented in Table I.

TABLE I
COMPOSITIONS OF THE INVESTIGATED RUBBER COMPOUNDS (PHR)

	E 1	E 2	E 3	E 4	E 5	E 6	E 7	E 8
ENR	100	100	100	100	100	100	100	100
ZnO	3.0	3.0	3.0	3.0	3.0	3.0	3.0	3.0
Stearic Acid	2.0	2.0	2.0	2.0	2.0	2.0	2.0	2.0
Carbon Black	50	70	…	…	20	20	…	…
Silica	…	…	70	70	50	50	…	…
PCSF	…	…	…	…	…	…	70	70
TESPT	…	…	…	7.0	…	5.0	…	5.0
TBBS	1.5	1.5	1.5	1.5	1.5	1.5	1.5	1.5
Sulphur	2.0	2.0	2.0	2.0	2.0	2.0	2.0	2.0

The rubber compounds were prepared at two stages according to the mixing schedule presented in Table II.

At the first stage the mixing was performed on a Brabender Plasti-Corder PLE651 fitted with a 300 cm^3 cam type mixer. The silane coupling agent was mixed with the filler studied prior to their placing into the mixer camera.

The amount of bis(triethoxysilylpropyl) tetrasulfide silane coupling agent (TESPT) used was 1 phr per 10 phr pure silica. At the second stage sulphur and the accelerator were added to the mixture compounded on an open two-roll laboratory mill L/D 320x160 and friction 1.27.

The vulcanization process of the natural rubber based compounds was carried out on an electrically heated hydraulic press using a special homemade mold at 150°C and 10 MPa.

III. Results and Discussion

III.1. Characterization of the Pyrolysed Carbon-Silica Filler (PCSF)

The investigated pyrolysed carbon-silica filler (PCSF) was obtained via pyrolysis-cum-water vapour of waste green tires tread (Michelin Energy 195/65 R15) by the method of L. Ljutzkanov [7] at the Institute of Chemical Engineering, Bulgarian Academy of Sciences.

TABLE II
MIXING SCHEDULE OF THE INVESTIGATED RUBBER COMPOUNDS

Mixing order	Ingredients	Mixing time, min	Cumulative time, min
Stage 1, Brabender Plasti-Corder PLE651, Rotor speed 40 rpm, Temperature 140ºC			
1	Epoxyprene 25	2	2
2	ZnO and stearic acid	2	4
3	Carbon black, silica or pyrolysed carbon-silica filler	5	9
Stage 2, Laboratory Two Roll Mills, Friction 1.27			
1	1st stage rubber batch	2	2
2	Sulphur and TBBS	5	7

Table III shows the ash content of the pyrolysed carbon silica filler to be about 64%, i.e. PCSF comprises about 36% of organic matter (carbon black) and 64% of inorganic compounds. The availability of some amounts of carbon black in PCSF allowed determining its iodine adsorption and oil absorption number. As seen, iodine adsorption of the pyrolysed carbon-silica filler is much higher than that of the conventional Corax N220 carbon black. That means the specific surface area of PCSF is larger than the one of Corax N220 carbon black; what has been also confirmed by BET (Brunauer–Emmett–Teller) nitrogen specific surface area. The primary particles formed during the stage of initial carbon black formation fuse together building up three dimensional branched clusters called aggregates. High structure carbon black has a high number of primary particles per aggregate, while low structure carbon black exhibits only a weak aggregation. These aggregates again may form agglomerates linked by Van der Waals interactions.

The empty space (void volume) between the aggregates and agglomerates, usually expressed as the volume of dibutylphthalate (DBP) absorbed by a given amount of carbon black, is described by the term "structure" (or "structurality") of the carbon black [10].

The data in Table III show the oil absorption number of PCSF to be significantly higher than that of the conventional carbon black. Hence, PCSF particles are able to form more pronounced secondary structures (aggregates and agglomerates). Since pyrolysed carbon-silica filler consists of about 64% of inorganic compounds, the ash contents of PCSF was characterized by silicate analysis (weight analysis, AAS and ICP-OES).

TABLE III
MAIN PROPERTIES OF THE FILLERS STUDIED

	Corax N220	Ultrasil 7000 GR	PCSF
Iodine adsorption (IA), mg/g	121	…	215
Oil absorption number (OAN), ml/100 g	114	…	140
Specific surface area (BET)[1], m^2/g	106	175	116
Ash content, %	<0.5	…	64
Mesopore volume, cm^3 (STP)[2]/g	…	…	91
Diameter of mesopores, nm	…	…	5

1 BET (Brunauer–Emmett–Teller)
2 STP – Standard temperature and pressure

Copyright © 2014 Praise Worthy Prize S.r.l. - All rights reserved

The data are presented in Table IV. As seen, PCSF contains mainly silica (SiO_2) (about 92.56%) and ZnO (about 3.82%), despite of the availability of many metal oxides (Al_2O_3, CaO, MgO, Na_2O, K_2O, Fe_2O_3, MnO, TiO_2, CuO, PbO, NiO and Cr_2O_3) in it. The result is expected having in mind that PCSF is the product from pyrolysis-cum-water vapour of waste green tires treads filled mainly with silica.

TABLE IV
ASH CONTENT OF THE PYROLYSED CARBON-SILICA FILLER ACCORDING TO THE SILICATE ANALYSIS, AAS AND ICP-OES

	Values, %
SiO_2	92.56
Al_2O_3	0.55
CaO	0.18
MgO	0.23
Na_2O	0.86
K_2O	0.08
Fe_2O_3	0.46
MnO	<0.01
TiO_2	0.02
ZnO	3.82
CuO	0.08
PbO	0.03
NiO	<0.01
Cr_2O_3	0.01

The ash content of the pyrolysed carbon-silica filler and its silicate analysis data allow the conclusion that PCSF contains about 60% of silica, 36% of carbon black, 2.5 % of zinc oxide and 1.5% of other metal oxides.

As said above, the silica surface is hydrophilic – it has silanol groups. The silanol groups could be isolated, geminal (two hydroxyl groups on the same silicon atom), and vicinal (on adjacent atoms). Generally they are linked by strong hydrogen bonds [11] causing aggregation of the filler particles. That hampers the filler dispersion in the rubber matrix as well as the formation of stable bonds between the elastomer and the filler.

Therefore the reinforcing effect of silica is less pronounced. A better dispersion of silica particles and stronger polymer-filler interactions are achieved using different types of silane coupling agents [4].

Bifunctional organosilanes are organic compounds which improve the compatibility between the hydrophobic polymer matrix and the hydrophilic silicon dioxide [12]. Bis (triethoxysilylpropyl) tetrasulfide (TESPT) is the most used of all and finds wide application in practice. During the mixing via hydrolysis and condensation the alkoxy groups of the bifunctional organosilane interact with the silanol groups of silica [13]-[16]. In the course of vulcanization the polysulfide groups of TESPT interact with the elastomer macromolecules [17], [18]. The polymer-filler bonds thus formed have a significant effect upon the properties of rubber composites. Lowered surface energy of silica leads to a higher rate of rubber adsorption onto the filler surface and to a weaker filler-filler interaction.

The aforementioned reveals the crucial role that silanol groups over the surface of silica have in the reinforcing process. So, it is of particular importance those groups to be preserved when silica filled rubber items undergo pyrolysis.

That is why both the pyrolysed carbon-silica filler and its ash contents were subjected to Fourier transform infrared (FTIR) spectroscopy (Figures 1(b) and 1(c)).

The FTIR spectrum of conventional silica (Ultrasil 7000 GR) presented in Fig. 1(a) is given for comparison.

As Figs. 1(b) and 1(c) show, the absorption bands of the pyrolysed carbon-silica filler and the ash content are in full accordance with that of the conventional silica (Fig. 1(a)). In all cases the following absorption bands have been observed: at 1200 - 1100 cm^{-1} – asymmetric valency vibrations of Si-O bonds; at 830 - 750 cm^{-1} – symmetric stretch vibrations of Si-O bonds; at 530 - 460 cm^{-1} – deformational vibrations of Si-O bonds; at 3600 – 3200 cm^{-1} – valency O-H vibrations assigned to hydrogen bonded OH groups; at 1660 – 1630 cm^{-1} – deformational O-H vibrations.

All spectra have well pronounced absorption bands at about 3400 cm^{-1} corresponding to the hydrogen bonding interactions associated with silanols, which are available on the surfaces of PCSF, of PCSF ash and of the silica filler [19]. According to FTIR spectroscopy data, the particles of silicon oxide that had been used as filler in tires manufacturing have preserved their chemical activity in the tires pyrolysis product.

The size of filler particles is of significant importance for its reinforcing effect. The smaller the particles, the more pronounced the reinforcing effect is. The morphology of the pyrolysed carbon-silica filler has been studied by transmission electron microscopy (TEM).

Figures 2 present the micrographs of conventional carbon black Corax N220 (Fig. 2(a)), conventional silica Ultrasil 7000 GR (Fig. 2(b)), pyrolysed carbon-silica filler (Fig. 2(c)) and the ash content of the pyrolysed carbon-silica filler (Fig. 2(d)).

Figs. 2 show that the particles of the conventional carbon black (50 nm) are much larger than those of the conventional silica which are about 20-25 nm. TEM micrograph of the pyrolysed carbon-silica filler shows that its particles size varies from 25 to 50 nm.

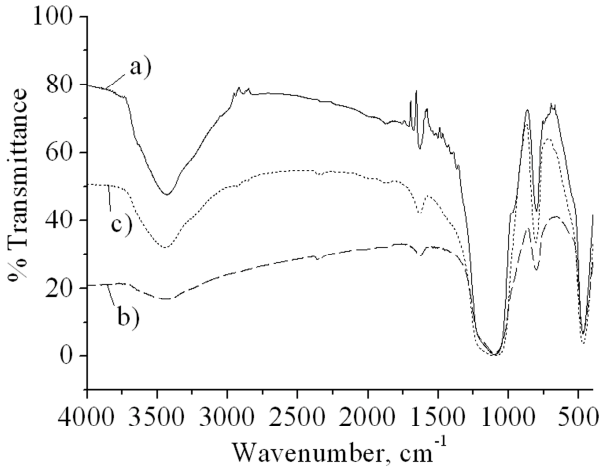

Figs. 1. FTIR spectra of the studied fillers: (a) Conventional silica (Ultrasil 7000GR); (b) Pyrolysed carbon-silica filler (PCSF); (c) The ash content of PCSF

Copyright © 2014 Praise Worthy Prize S.r.l. - All rights reserved

That means PCSF particles are of almost the same size as the particles of conventional carbon black and conventional silica. However, Fig. 2(d) shows that the ash of the PCSF has particles of uniform size which is commensurable with the size of the particles of conventional silica (about 20-25 nm). According to TEM analysis the particles size of pyrolysed carbon-silica filler is commensurable with that of the conventional fillers used in rubber industry.

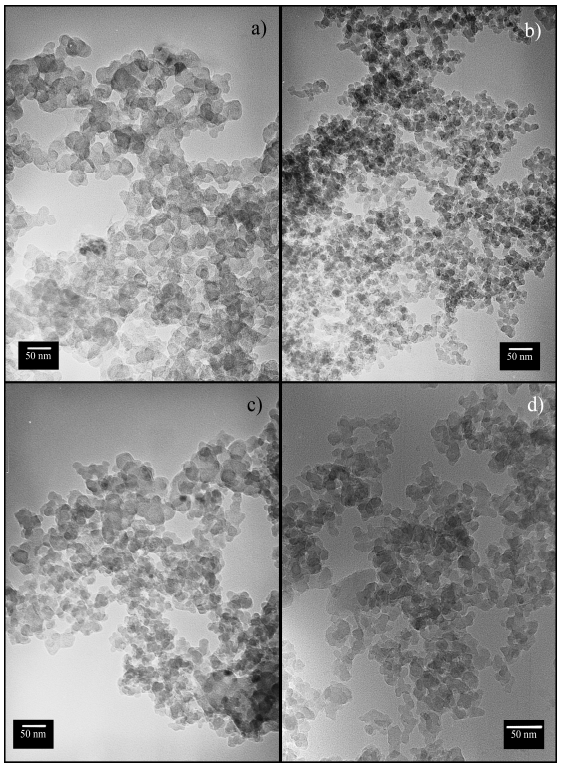

Figs. 2. TEM micrographs of the investigated fillers: (a) Corax N220 (x100k); (b) Ultrasil 7000 GR (x100k); (c) Pyrolysed carbon-silica filler (x100k); (d) The ash content of pyrolysed carbon-silica filler (x150k)

III.2. Curing Properties of the Investigated Rubber Compounds

Table V summarizes the main curing properties of the rubber compounds studied as determined from their cure curves presented in Fig. 3.

As seen from Table V, the increase in the amount of Corax N220 carbon black from 50 phr to 70 phr leads to a regular increase in the minimum torque (ML), in the viscosity of the studied rubber composites, respectively. ML of the composite comprising Corax N220 at 50 phr (E 1) is 1.69 dNm, while that of the composite with Corax N220 (E 2) at 70 phr it is 4.84 dNm. Obviously, the amount of carbon black does not affect considerably the scorch time (T_{s2}) and the cure time (T_{90}) of those two composites. ML of the composite filled with conventional silica Ultrasil 7000 GR at 70 phr without a silane coupling agent (E 3) is 15.88 dNm and is quite higher than that of the composite comprising the same amount of carbon black (E 2).

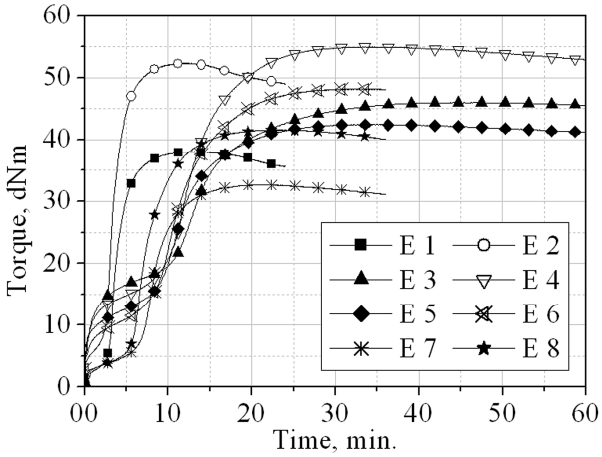

Fig. 3. Cure curves of the investigated rubber compounds taken at 150ºC

TABLE V
CURING PROPERTIES OF THE INVESTIGATED RUBBER COMPOUNDS

	Min ML, dNm	Max ML, dNm	ΔM, dNm	T_{s2}, min:s	T_{90}, min:s	Cure Rate, %/min
E1	1.69	38.02	36.33	2:11	6:12	25.0
E2	4.84	52.31	47.47	2:00	5:45	26.7
E3	15.88	46.04	30.16	9:00	27:30	5.4
E4	12.86	55.00	42.14	8:06	20:04	8.3
E5	11.18	42.50	31.32	7:30	20:00	8.0
E6	8.82	48.19	39.37	6:30	20:00	7.4
E7	2.59	32.66	30.07	4:18	12:23	12.1
E8	2.50	41.61	39.11	3:02	12:13	10.8

In the presence of TESPT at 7 phr (E 4), ML values of the rubber composites filled with Ultrasil 7000 GR decrease about 20% and reach 12.86 dNm. In the case neither the presence nor the lack of TESPT has a significant effect upon the scorch time (T_{s2}) and the cure time (T_{90}). Though, it is obvious that the scorch time (T_{s2}) and the cure time (T_{90}) are much longer than those of the rubber compounds filled with carbon black (E 1, E 2). Naturally, that has been expected having in mind that the curing agents are being adsorbed over silica surface which lowers the vulcanization rate. What has been said about ML values, the scorch time (T_{s2}) and the cure time (T_{90}) of the rubber compounds filled with conventional silica (E 3, E 4) is valid for the rubber compounds filled with a combination of conventional silica and carbon black (E 5, E 6).

The presence or absence of a silane coupling agent does not lead to changes in ML values for the rubber compounds comprising a pyrolysed carbon-silica filler (E 7, E 8). In the case the scorch time (T_{s2}) and the cure time (T_{90}) also do not change significantly because of the presence or lack of TESPT. As seen, ML values of the rubber compounds comprising a pyrolysed carbon-silica filler both with and without TESPT are about 70-80% lower than those of the respective compounds filled with conventional silica (E 3, E 4) or with a combination of conventional silica and carbon black (E 5, E 6).

Meanwhile the scorch time (T_{s2}) and the cure time (T_{90}) are considerably shorter.

Copyright © 2014 Praise Worthy Prize S.r.l. - All rights reserved

Possibly the product yielded from the pyrolysis-cum-water vapour of waste green tires tread is similar to the dual-phase fillers CSDPF 2000 and CSDPF 4000 developed by Cabot Corporation.

According to literature the filler-filler interactions in rubber compounds comprising similar fillers is less pronounced than in the case when the rubber compounds are filled with a physical mixture of carbon black and silica [2].

On its turn that leads to better dispersion of the filler particles along the rubber matrix and to lower viscosity of the rubber compounds investigated. As Table V shows, in all cases the presence of a silane coupling agent has not a very pronounced effect upon the viscosity of the rubber compounds filled with silica (E 3 to E 8).

That is due to the polar character of the epoxidized natural rubber (Epoxyprene 25). Epoxidation of natural rubber increases the polarity of the polymer. That is why the interaction between epoxidized natural rubber and silica is stronger and there is no need of coupling agents [3].

III.3. Mechanical Properties of the Investigated Rubber Composites

Table VI presents the mechanical properties of the studied Epoxyprene 25 based rubber composites.

TABLE VI
MECHANICAL PROPERTIES OF THE INVESTIGATED RUBBER COMPOSITES

	M_{100}, MPa	M_{300} MPa	σ, MPa	ε_1, %	ε_2, %	Shore A hardness	Abrasion, mm^3
E1	3.5	16.8	25.8	420	30	75	130
E2	5.1	24.4	24.8	300	20	82	139
E3	3.7	14.1	16.5	300	10	80	150
E4	3.5	17.2	22.9	360	10	81	128
E5	4.1	20.4	21.9	320	10	77	137
E6	4.7	22.8	25.3	300	10	81	126
E7	3.8	18.8	23.8	420	25	76	137
E8	4.3	21.7	25.0	345	20	77	129

As Table VI, shows Modulus 100 (M_{100}) of the composites filled with Corax N220 carbon black (E 1) at 50 phr is about 3.5 MPa. M_{100} of the composites filled with Corax N220 carbon black (E 2) at 70 phr is about 5.1 MPa or about 45% higher than that of the former composite, E 1. Modulus 300 (M_{300}) of composites E 1, E 2 also increases about 45% with the increasing filler amount.

The tensile strength (σ) values of the composites filled with carbon black (E 1, E 2) is about 25-26 MPa, i.e. the increase in the filler amount from 50 phr to 70 phr does not affect much this parameter. However, the increase in the carbon black amount causes a decrease of the values of elongation at break (ε_1) and residual elongation (ε_2), while Shore A hardness and abrasion values increase.

The presence of a coupling agent has no significant effect upon M_{100} values of the composites filled with conventional silica Ultrasil 7000 GR (E 3, E 4), a combination of conventional silica and carbon black (E 5, E 6) or with pyrolysed carbon-silica filler (E 7, E 8).

Though, in all three cases, the presence of TESPT leads to an increase in M_{300} and tensile strength values and to lowering the abrasion. The mechanical properties of the composites comprising pyrolysed carbon-silica filler (E 7, E 8) are commensurable with those of the composites with conventional fillers.

The mechanical properties of the composites comprising pyrolysed carbon-silica filler and an organosilane are improved due to the occurrence of chemical polymer-filler interactions. Such interactions can proceed naturally, if under the chosen the pyrolysis conditions the particles of silica preserve their primary size and surface activity what has been confirmed by the data obtained via FTIR and TEM analyses.

III.4. Dynamic Properties of the Investigated Rubber Composites

Filler dispersion along the rubber matrix has a significant impact upon the dynamic properties of the vulcanizates and mainly upon their heat build-up - a property related to tires rolling resistance. A flexometer Goodrich was used to determine the dependencies of the complex dynamic modulus (E*) and heat build-up on the dynamic deformation.

Fig. 4 presents the complex dynamic modulus (E*) dependence on the dynamic deformation of the studied Epoxyprene 25 based composites. As the figure shows, at all studied deformations the dynamic complex modulus values of the composites comprising carbon black (E 1, E 2) increase with increasing the filler amount from 50 phr to 70 phr. In the case of the composites comprising carbon black at 70 phr (E 2), however, the drop of the complex dynamic modulus (E*) values at higher dynamic deformation (Payne effect) is more pronounced.

That is due to the fact that at higher filler amounts the interactions between its particles are stronger.

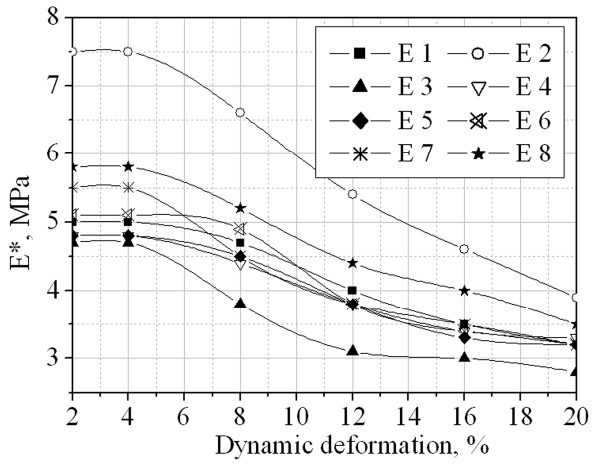

Fig. 4. Dependence of the complex dynamic modulus of the composites studied on the dynamic deformation

Copyright © 2014 Praise Worthy Prize S.r.l. - All rights reserved

At low dynamic deformation values (up to 8%), the filler-filler interactions remain the same and the dynamic complex modulus values (E*) are relatively high. At higher dynamic deformations the filler-filler structure is destroyed and the dynamic complex modulus values decrease. That corresponds to a higher heat build-up.

As seen from Fig. 4, at all studied deformations the composites comprising conventional silica Ultrasil 7000 GR and no coupling agent (E 3) have the lowest dynamic complex modulus values. In the case of the composite comprising Ultrasil 7000 GR (E 4) the presence of TESPT leads to a significant increase in the dynamic complex modulus values, while E* values decrease less with the increasing dynamic deformation.

The same is valid for the complex dynamic modulus (E*) values of the composites comprising a combination of conventional silica and carbon black (E 5, E 6), as well as for those of the composites comprising a pyrolysed carbon-silica filler (E 7, E 8). At all studied deformations the complex dynamic modulus (E*) values of the composites comprising a pyrolysed carbon-silica filler in the presence of TESPT (E 8) are the highest compared to the values of all studied silica filled composites.

Fig. 5 plots the heat build-up as a function of the dynamic deformation of the epoxidized natural rubber composites studied. The figure shows the heat build-up data to be in full accordance with those about the complex dynamic modulus (Figure 4). As seen, in the presence of TESPT the composites filled with conventional silica Ultrasil 7000 GR (E 4), a combination of silica and conventional carbon black Corax N220 (E 6), as well as those with a pyrolysed carbon-silica filler (E 8) have heat build-up values lower than those of the composites comprising no coupling agent.

The heat build-up values of the composites comprising pyrolysed carbon-silica filler are commensurable with those of the composites comprising conventional fillers. Dynamic mechanical testing is a powerful predictive tool that can provide valuable insight into the tire performance of tread compounds.

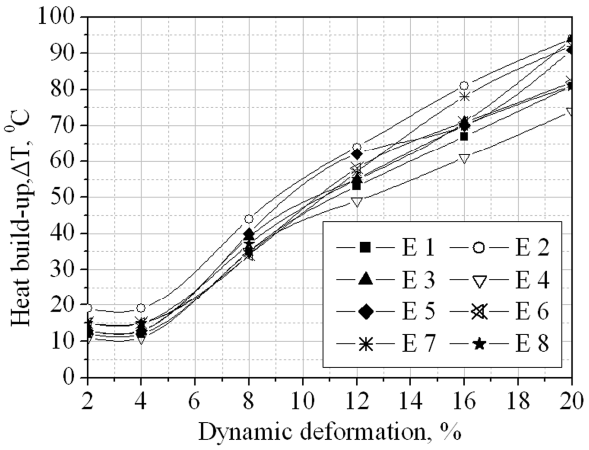

Fig. 5. Dynamic deformation dependence of the heat-build up of the composites studied

Certain tire tread characteristics correlate with the mechanical dynamic properties measured on a Dynamic mechanical thermal analyzer (DMTA) under defined frequency, strain (or stress) conditions, and temperature.

The instrument can be used to differentiate instantly a series of tested compounds [20].

Tire tread deformation during motion under load has been described as consisting of predominantly bending strains in which the curved tread is bent inwards and outwards as a function of the contact region. The total strain is composed primarily of the tangential strain in the plane of the tire and the shear strain between the radial and tangential directions. Strain and stress amplitudes depend on the magnitude of tire deflection.

Medalia has put forth that the tread deformation can be resolved approximately into constant strain (bending) and constant stress (compression) conditions.

Tension-compression, shear and torsional deformations are often utilized to test tire tread formulations under dynamic conditions. As a viscoelastic property tan δ deserves interest being in correlation with rolling resistance (due to hysteresis causing heat build-up) and to wet grip characteristics [20].

Fig. 6 presents the dependence of the dynamic storage modulus (E') on temperature. According to the figure all studied composites are in the glass state in the range from -80ºC to -30ºC. In the said temperature interval there are no considerable differences in the storage modulus values depending on the type of used filler or on the presence or absence of silane coupling agent.

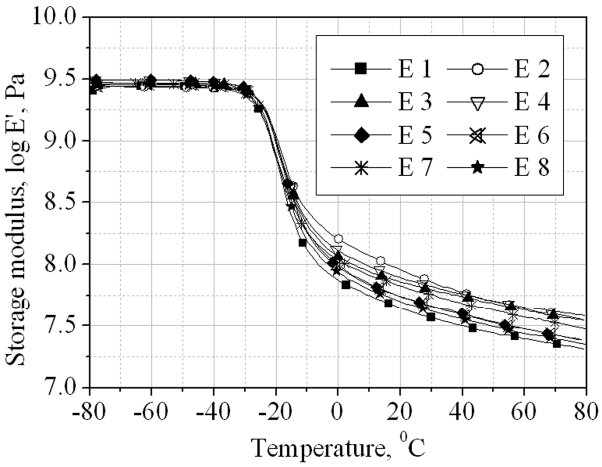

Fig. 6. Storage modulus (E') dependency on the temperature of the investigated composites

The considerable differences in storage modulus values are observed in the range from -10ºC to 80ºC, wherein the studied composites are in the viscoelastic state. In the said temperature interval the increase in the carbon black amount from 50 phr (E 1) to 70 phr (E 2) leads to higher storage modulus values of the composites studied. All composites comprising conventional silica Ultrasil 7000 GR (E 4), a combination of silica and Corax N220 carbon black (E 6) or pyrolysed carbon-silica filler (E 8) in presence of TESPT have storage

Copyright © 2014 Praise Worthy Prize S.r.l. - All rights reserved

modulus values higher than those of the composites without a silane coupling agent.

Tan δ being the ratio between the dynamic loss modulus (E'') and dynamic storage modulus (E') (tan δ = E''/E') illustrates the macromolecules mobility as well as the phase transitions in the polymers. The temperature dependence of tan δ values deserves interest since it is considered that tan δ at 60ºC corresponds to the tires rolling resistance while tan δ at 0ºC – to the wet road grip of the tires. Fig. 7 presents the temperature dependence of the mechanical loss angle (tan δ) of the composites studied. The figure does not show that the type of filler or organosilane used causes a significant difference in tan δ values of the composites at 0ºC and 60ºC.

The exception are the vulcanizates comprising carbon black at 70 phr (E 2) whose tan δ values at 0ºC are the lowest while those at 60ºC are the highest. In the case the wet road grip would be lower and the rolling resistance would be higher than that of the composites comprising conventional silica, a combination of silica and carbon black or pyrolysed carbon-silica filler.

The improved mechanical and dynamic properties of the composites comprising pyrolysed carbon-silica filler in the presence of organosilane are due to the formation of chemical bonds between the polymer and the filler.

Such interactions are possible only provided that under the chosen pyrolysis conditions in the presence of organosilane the silica particles preserve their primary particle size and surface activity. That has been confirmed by the FTIR and TEM analyses. May be the product obtained via pyrolysis-cum-water vapour of waste green tires tread is similar to the dual phase fillers CSDPF 2000 and CSDPF 4000 developed by Cabot Corporation. The filler-filler interaction in the rubber compounds comprising such fillers is markedly lower than that of the rubber compounds filled with a physical mixture of carbon black and silica. That leads to a better dispersion of the filler particles along the rubber matrix and to stronger polymer-filler bonds, what results into a more pronounced reinforcing filler effect.

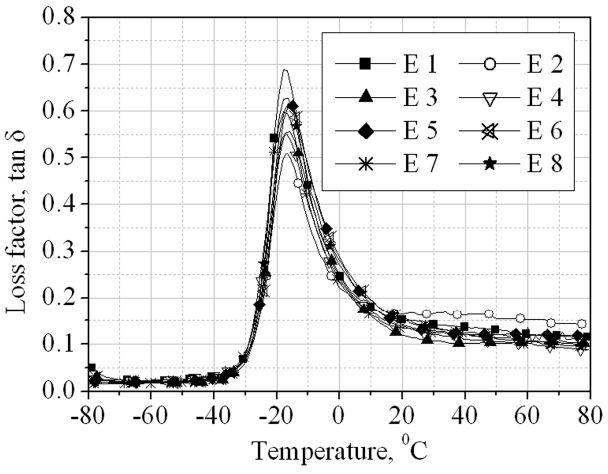

Fig. 7. Mechanical loss angle tangent (tan δ) dependency on the temperature of the investigated composites

The analyses reported herein do not give a certain answer whether the pyrolysed product obtained is a dual phase filler of the carbon-silica type or a mechanical mixture of those two components.

The search of a definite answer to the question is going to be the scope of our future studies. The results obtained allow considering the pyrolysed carbon-silica filler tantamount to the conventional silica filler when used to develop elastomer composites based on epoxidized natural rubber.

IV. Conclusion

The ash content of the pyrolysed carbon-silica filler (PCSF) yielded from pyrolysis-cum-water vapour is about 64%, i.e. PCSF consists of 36% of organic matter (carbon black) and 64% of inorganic compounds. It has been determined by weight analysis, AAS and ICP-OES that the ash content of PCSF comprises 92.56% of silica, 3.82% of zinc oxide and 3.62% of other metal oxides.

The results obtained show that PCSF consists of 60% of silica, 36% of carbon black, 2.5% of zinc oxide and of about 1.5% of Al_2O_3, CaO, MgO, Na_2O, K_2O, Fe_2O_3, MnO, TiO_2, CuO, PbO, NiO and Cr_2O_3.

The pyrolysis conditions turned to be a major factor for preserving particle size and surface chemical activity of silica and carbon black used as fillers in tires in the pyrolysed product.

The vulcanization characteristics, mechanical and dynamic properties of composites based on epoxidized natural rubber reinforced with the pyrolysed carbon-silica filler (PCSF) have been studied.

The data obtained have been compared to those about analogous composites comprising conventional fillers. It has been established that the vulcanization characteristics, mechanical and dynamic properties of the studied rubber compounds and vulcanizates filled with PCSF are commensurable, even in some cases they are improved compared to those of the composites comprising the conventional fillers. The presence or absence of TESPT does not affect significantly the properties of the composites studied. That is on account of the polar character of epoxidized natural rubber which forms strong bonds with silica even without a compatibilizer.

All said above allows the conclusion that conventional fillers silica and carbon black could be replaced totally by PCSF in manufacturing rubber compounds and vulcanizates of epoxidized natural rubber.

Acknowledgements

The present research is a result of an international collaboration program between University of Tabuk, Tabuk, Kingdom of Saudi Arabia and the University of Chemical Technology and Metallurgy, Sofia, Bulgaria.

The authors gratefully acknowledge the financial support from the University of Tabuk.

Copyright © 2014 Praise Worthy Prize S.r.l. - All rights reserved

References

[1] C. M. Flanigan, L. Beyer, D. Klekamp, D. Rohweder, B. Stuck and E.R. Terrill, Comparative study of silica, carbon black and novel fillers in tread compounds, *Rubber World 245 (2012) 18-31*.

[2] M. J. Wang, Y. Kutsovsky, P. Zhang, G. Mehos, L. J. Murphy and K. Mahmud, Using carbon-silica dual phase filler improve global compromise between rolling resistance, wear resistance and wet skid resistance for tires, *Kaut. Gummi Kunstst. 55 (2002) 33-40*.

[3] A.V. Chapman, Natural rubber and NR-based polymers – renewable materials with unique properties, *24th International H.F. Mark-Symposium, Advances in the Field of Elastomers & Thermoplastic Elastomers, Vienna, Austria, November 15-16 (2007).*

[4] E. M. Dannenberg, (1981) Filler choices in the rubber industry the incumbents and some new candidates, *Elastomerics 113 (1981) 30–50.*

[5] G. Mazloom, F. Farhadi and F. Khorasheh, Kinetic modeling of pyrolysis of scrap tires, *J. Anal. Appl. Pyrol. 84 (2009) 157-164*.

[6] J. Shah, Jan M. Rasul , F. Mabood and M. Shahid Conversion of waste tyres into carbon black and their utilization as adsorbent, *J. Chinese Chem. Soc., 53 (2006) 1085-1089*.

[7] L. Ljutzkanov, Method of processing carbon containing materials, Patent 63594/26.02.2002, Republic of Bulgaria.

[8] M. Ivanov and M. Mihaylov, Silica obtained via pyrolysis of waste "green" tyres – a perspective filler for rubber industry, *Kaut. Gummi Kunstst, 63, (2010) 303-307.*

[9] M. Ivanov and M. Mihaylov, Silica obtained via pyrolysis of waste "green" tyres – a filler for tyre tread rubber blends, *J. Elastom. Plast., 43, (2011) 303-316.*

[10] W. Niedermeier, J. Fröhlich and H. D. Luginsland, Reinforcement mechanism in the rubber matrix by active fillers, *Kaut. Gummi Kunstst, 55, (2002) 356-366.*

[11] B. Rodgers and W. Waddell In: *The Science and Technology of Rubber*, 4th edn. , (Elsevier Inc., 2013)

[12] L. R. Evans and W. H. Waddell, Ultra-high reinforcing precipitated silica for tire and rubber applications, *Kaut. Gummi Kunstst., 48, (1995) 718-723.*

[13] S. Wolff, Silanes in tire compounding after ten years – a review, *Tire Sci. Tech., 15, (1987) 276-294*.

[14] A. Hunsche, U. Görl, A. Müller, M. Knaack and T. Göbel, Investigations concerning the reaction silica/organosilane and organosilane/polymer - part 1: Reaction mechanism and reaction model for silica/organosilane, *Kaut. Gummi Kunstst., 50, (1997) 881-889*.

[15] A. Hunsche, U. Görl, H. G. Koban and T. Lehmann, Investigations on the reaction silica/organosilane and organosilane/polymer - part 2. Kinetic aspects of the silica-organosilane reaction, *Kaut. Gummi Kunstst., 51, (1998) 525-533*.

[16] U. Görl, A. Hunsche, A. Müller and H. G. Koban, Investigations into the silica/silane reaction system, *Rubber Chem. Technol., 70, (1997) 608-623.*

[17] U. Görl and A. Parkhouse, Investigations on the reaction silica/organosilane and organosilane/polymer part 3: investigations using rubber compounds, *Kaut. Gummi Kunstst., 52, (1999) 493-500.*

[18] U. Görl, J. Münzenberg, D. Luginsland and A. Müller, Investigations on the reaction silica/organosilane and organosilane/polymer - part 4: studies on the chemistry of the silane sulfur chain, *Kaut. Gummi Kunstst., 52, (1999) 588-593*.

[19] S. Siriwardena, H. Ismail and U. Ishiaku, A Comparison of white rice husk ash and silica as fillers in ethylene-propylene-diene terpolymer vulcanizates, *Polym. Int., 50 (2001) 707-713*.

[20] J. E. Martens, E. R. Terrill, J. T. Lewis, R. J. Pazur and R. Hoffman, Effect of deformation mode in prediction of tire performance by dynamic mechanical analysis, Rubber World, 248, (2013) 29-35.

Authors' information

[1]Department of Physics,
Faculty of Science,
King Abdulaziz University,
Jeddah 21589,
Saudi Arabia.

[2]Department of Polymer Engineering,
University of Chemical Technology and Metallurgy,
8 Kl. Ohridski blvd., 1756 Sofia,
Bulgaria.

[3]Institute of Chemical Engineering,
Bulgarian Academy of Sciences,
1113 Sofia, Bulgaria.

Copyright © 2014 Praise Worthy Prize S.r.l. - All rights reserved

Praise Worthy Prize

International Review of Chemical Engineering (I.RE.CH.E.), Vol. 6, N. 4
ISSN 2035-1755 *July 2014*

Computer Simulation and Parametric Analysis of an Old Ammonia Industrial Storage Unit

Alessandra Caldas d' Moraes Elisiario, Adilson José de Assis

Abstract – *Old chemical plants are still used worldwide mainly in commodities production. These facilities usually hold performance standards and operational points different from original design, which impacts in loss of energetic efficiency and even in products with unsatisfactory quality. Computer simulation nowadays represents a valuable tool when the objective is the optimization of these units. This work aimed the analysis of an ammonia industrial storage unit through computer simulation using COCO, a free-of-charge computer simulator, based on the CAPE-OPEN protocol. Through the simulation of the original design conditions of the unit, it was possible to verify that COCO and the Peng-Robinson Equation of State achieved good accuracy. Using parametric analysis we show that the pressure specification of the received ammonia does not have any influence on the other process variables of the industrial unit. On the other hand, the elevation of the operational pressure of the storage spheres increases the temperature of the exported ammonia in 6 K. This elevation increases the ammonia's vapor pressure, its tendency to volatilize and causes pump cavitation. Through simulation, a new operational point was proposed. We show that it is possible to obtain an energetic gain of 28.61 kW at the pumps and compressors when comparing to the current operational point. This gain corresponds to an energy cost reduction of 3.34% in this equipment. Under this new condition, the temperature of the exported ammonia can be returned to its original designed value.* ***Copyright © 2014 Praise Worthy Prize S.r.l. - All rights reserved.***

Keywords: *Computer Simulation, CAPE-OPEN Chemical Simulators, Fertilizers, Ammonia Storage*

I. Introduction

The production of commodities at industrial scale is commonly performed in old chemical plants worldwide [1]-[11].

These industrial facilities normally have operational points and performance standards different from those originally designed, which impacts in loss of energetic efficiency and even in products with unsatisfactory quality. Computer simulation represents a valuable tool nowadays when the objective is the optimization of these units, once it enables to predict different operational conditions up to the best point before implementing the changes in the actual industrial facility.

The "Triângulo Mineiro" region, in Minas Gerais state, Brazil, is an important fertilizer producer hub. Triple superphosphate, simple superphosphate and monoammonia phosphate are examples of the fertilizers produced at this location. The last one, also known as MAP, is produced by the reaction between phosphoric acid and ammonia.

The ammonia used is not produced at this fertilizer facility. It is received by trucks and stored at a thirty-four-year-old industrial unit that contains heat exchangers, compressors, pumps, flash vessels, storage spheres, etc.

Due to changes over time in the specification of the ammonia supply, and to operational conditions different from those designed for the storage unit, there are frequently maintenance problems, gain of energetic efficiency opportunities and issues on the quality of the ammonia sent to the MAP production units. Fig. 1 shows a typical ammonia storage unit that uses flash vessel, heat exchangers, compressors, pumps, and spheres. This storage unit was taken into account in this work.

Considering this scenario, the overall objective of this study was the simulation of the ammonia industrial storage unit with the aid of COCO [2], a free-of-charge chemical process simulator, based on the CAPE-OPEN protocol. First, we simulated the process in order to reproduce original design conditions. After that, the current operational data were also simulated, and it was found through parametric analysis that the specification of the received ammonia does not have any influence on the other process variables of the industrial unit.

On the other hand, the elevation of the operational pressure of the storage spheres increases the temperature of the ammonia exported to the MAP facilities, which elevates the ammonia's vapor pressure, its tendency to volatilize and causes pump cavitation. COCO was also used to analyze the process sensibility to variables set-point changes.

Copyright © 2014 Praise Worthy Prize S.r.l. - All rights reserved

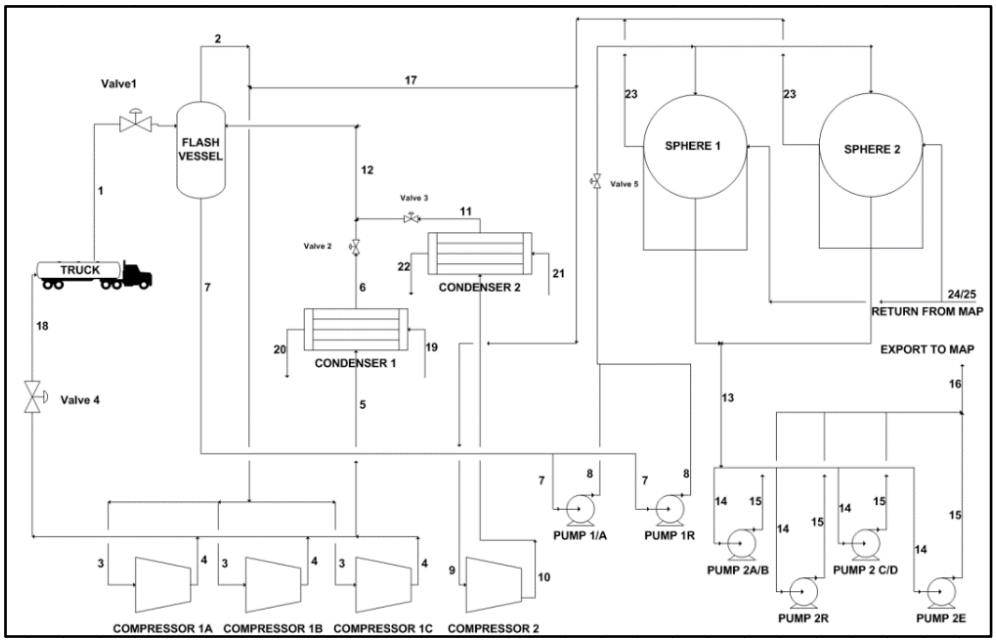

Fig. 1. Process flow diagram of the ammonia storage unit considered in this work
Source: FERTILIZER COMPANY, [4]

Through simulation, a new operational point was proposed and it was possible to obtain energetic gains at the pumps and compressors. Under this new condition, the temperature of the ammonia sent to the MAP units can be returned to its original design values.

II. Literature Review

II.1. Chemical Process Simulation with COCO (CAPE-OPEN to CAPE-OPEN) Simulator

Process simulation is largely used for the development, analysis, synthesis and optimization of chemical processes, without interfering with the operational safety of the industrial unit [1]. It is also applied at operation training and environmental emissions estimations.

CAPE stands for *Computer Aided Process Engineering*. CAPE-OPEN [3] is a collection of open software interface standards that describe the interaction between flowsheet software components [11]. It is a protocol for software interface elaboration that allows a standardized communication between different process simulators and third-part developed products.

This communication is free-of-charge and opened to contributions.

It is the formal documentation that includes areas such as unit operations, physical properties and numerical solvers. The COCO Simulator [2] is a free-of-charge, non-commercial, graphical, modular and CAPE-OPEN compliant, steady-state, sequential simulation process modeling environment. It was originally intended as a test environment for CAPE-OPEN modeling tools but now provides free chemical process simulation for everyone. It is an open flowsheet modeling environment allowing anyone to add new unit operations or thermodynamics packages.

II.2. Ammonia

Ammonia is an important fluid, and it is among the ten chemicals produced in greater quantities in the world.

It has a high enthalpy of vaporization, which gave to this fluid a prominent role as a refrigerant in the history of the industry. Over the years, the consumption of ammonia as a refrigerant has been superseded by its utilization in the agricultural fertilizers industry, mainly due to safety issues. Synthetic ammonia has become the main source of nitrogen for all fertilizers since 1945 [6].

Ammonia is a polar substance with a significant dipole moment, which gives it a behavior that differs substantially from nonpolar substances. Due to this behavior, the models that best represent chemical processes containing this fluid are based on the Soave-Redlich-Kwong or Peng-Robinson Equation of State [9].

A large part of the ammonia produced worldwide is transported from its production sites to its consumers' facilities, where it is used as raw-material for the remaining stages of the fertilizers consumption stages.

This transport is necessary because, normally, the availability of natural gas, raw material for the production of ammonia, is not near the phosphate rocks mines. Ammonia is usually transported in its liquid state, so, it needs to be compressed or cooled, because at room temperature, ammonia is a gas. The boiling temperature of ammonia varies from 240.15 K at sea level to 235.15 K at an altitude of 1,100 m.

The first tanks designed for the storage of ammonia used the concept of ammonia pressurization, in order to enable its storage at room temperature.

Copyright © 2014 Praise Worthy Prize S.r.l. - All rights reserved

However, these vessels only stores up to 400 ton of ammonia and were substituted over the years by cooled tanks that store ammonia at room pressure, which allowed the storage of quantities over 4,000 tons of this chemical [7]. The storage of intermediate quantities of ammonia, between 400 and 4,000 tons, is held in semi-pressurized and semi-refrigerated spheres [10].

III. Methodology

The software employed for the development of this study was the version 2.05 of the COCO simulator.

This work was divided in four steps: validation of the thermodynamic packages used in the simulation; construction of the process flowsheet and simulation of the project data of the industrial unit; simulation of the current operational data of the unit and parametric analysis of the variables; and proposal of a new adjusted operational point.

IV. Results and Discussion

IV.1. Thermodynamic Validation

The thermodynamic models chosen as candidates to be used in the simulations were Soave-Redlich-Kwong and Peng-Robinson Equation of States (EOS), as previously stated in the literature review. Values of Enthalpy, or H, Entropy, or S, and Specific Volume, or V, were calculated using these models.

The simulated results were compared to literature data available at Moran e Shapiro[8].

The pressure and temperature range used in the validation were chosen according to the ranges present at the industrial unit.

The equation chosen to be used at this work was Peng-Robison, based on the average error results, shown at Table I.

TABLE I
ERRORS OF THE THERMODYNAMIC VALIDATION

	Relative error using Peng-Robinson EOS (%)	Relative error using Soave-Redlich-Kwong EOS (%)
Specific Volume (m^3/kg)	1.34	1.55
Enthalpy (kJ/kg)	4.12	4.72
Entropy (kJ/kg.K)	4.1	4.72
Average Error (%)	3.19	3.66

IV.2. Simulation of the Original Design Data of the Industrial Unit

The process flowsheet simulated using COCO is shown at Fig. 2 and Table II shows the error between simulated and design data. From the results, it can be seen that the simulator could reproduce very well the design conditions.

IV.3. Simulation of the Current Operational Data of the Unit

The simulation of the current operational data of the industrial unit was performed with the same COCO flowsheet, since no structural change was made at the unit over the years. Some of the input parameters for pressure and temperature were altered according to the current operational conditions, as shown at Table III.

In order to better understand the impact of the operational changes on other key process parameters, a parametric analysis was made, as follows:

Pressure of the truck

It was observed that the alteration of the truck´s temperature and pressure does not have any impact on the other process variables (results not shown here).

TABLE II
ORIGINAL DATA DESIGNED TO THE PROCESS FLOW DIAGRAM (PFD) AND SIMULATED RESULTS COMPARISON

Stream	T (K)			P abs (kPa)			Mass Flow (t/h)		
	PFD	COCO	Error (%)	PFD	COCO	Error (%)	PFD	COCO	Error (%)
1	318.15	318.15	0.00%	1,760.28	1,760.29	0.00%	37.50	37.50	0.00%
2	263.15	262.49	-0.25%	281.44	281.44	0.00%	9.49	9.49	0.00%
4	413.15	413.15	0.00%	1,662.22	1,662.22	0.00%	3.16(x3)	9.49	0.00%
5	413.15	413.15	0,00%	1,662.22	1,662.22	0.00%	9.49	9.04	-4.74%
6	316.15	316.15	0.00%	1,662.22	1,662.22	0.00%	9.49	9.04	-4.74%
7	263.15	262.49	-0.25%	281.44	281.44	0.00%	38.00	37.54	-1.21%
8	263.15	262.56	-0.22%	568.78	568.78	0.00%	38.00	37.54	-1.21%
9	264.15	263.16	-0.38%	289.29	289.29	0.00%	0.45	0.45	0.00%
10	413.15	411.82	-0.32%	1,662.22	1,662.39	0.01%	0.45	0.45	0.00%
11	316.15	316.15	0.00%	1,662.22	1,662.39	0.01%	0.45	0.45	0.00%
12	263.15	263.15	0.00%	281.44	281.44	0.00%	9.94	9.48	-4.63%
13	264.15	263.47	-0.26%	289.29	289.29	0.00%	37.00	37.05	0.14%
15	264.15	263.47	-0.26%	1,466.09	1,466.09	0.00%	37.00	37.05	0.14%
18	413.15	409.67	-0.84%	1,269.95	1,269.95	0.00%	0.45	0.45	0.00%
19	303.15	303.15	0.00%	387.35	387.35	0.00%	872.00	872.00	0.00%
20	307.15	303.78	-1.10%	289.29	289.29	0.00%	872.00	872.00	0.00%
21	303.15	303.15	0.00%	387.35	387.35	0.00%	21.00	21.00	0.00%
22	311.15	304.48	-2.14%	289.29	289.29	0.00%	21.00	21.00	0.00%

Copyright © 2014 Praise Worthy Prize S.r.l. - All rights reserved

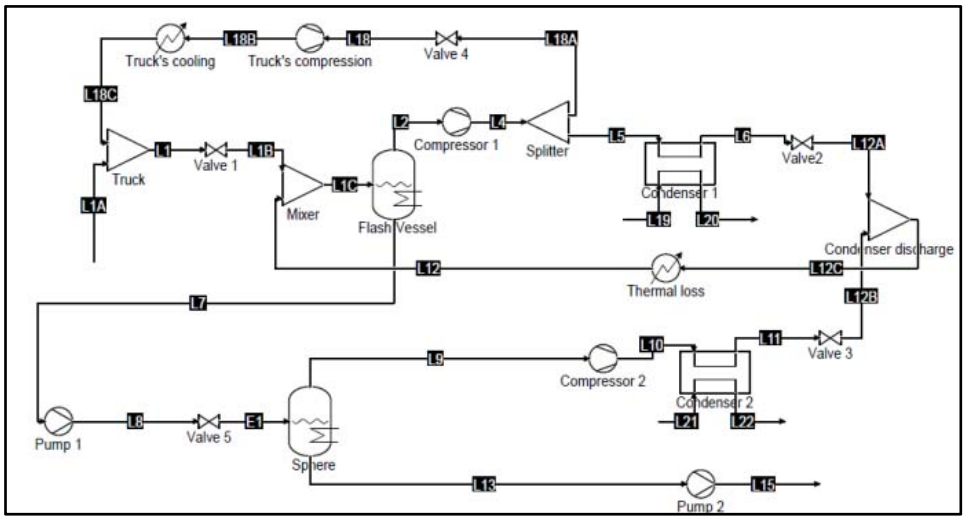

Fig. 2. Process flowsheet simulated with COCO

TABLE III
PROCESS VARIABLES ALTERATIONS

Stream	Equipment	Design data	Current operational data
1	Truck	318.15K and 1,760.28 kPa	298.15 K and 1,122.85 kPa
2	Flash vessel	281.44 kPa	318.71 kPa
4	Compressor 1	1,662.22 kPa	1,564.15 kPa
7	Flash vessel	281.44 kPa	318.71 kPa
23	Sphere	289.29 kPa	367.74 kPa

Source: FERTILIZER COMPANY [4]

Pressure of the flash vessel

The parametric analysis of the pressure of the flash vessel showed that it has a direct impact on the operational temperature of the vessel, and therefore on the energy consumptions of compressor and pump 1, as shown at Figs. 3 to 5. The dependence of the operating pressure and temperature of the flash vessel is a direct consequence of thermodynamics. The phenomenon of flash represents the vaporization of part of a determined fluid, which occurs at a certain pressure, with a correspondent saturation temperature. Each pressure has a correlated temperature, and the higher the pressure, the greater its saturation temperature. From Figs. 4 and 5 it is possible to observe that, the higher the pressure of the flash vessel, the lower the energy consumption of both compressor and pump 1.

This occurs because, when the flash vessel outlet stream has a higher pressure, it is more compressed. As a consequence, the necessity of pressure elevation done by the equipment is smaller, and so the energy consumption.

Pressure of the spheres

The parametric analysis of the pressure of the spheres showed that it has a direct impact on the operational temperature of the spheres, on the energy consumptions of compressor and pump 2 and on the ammonia export temperature to the MAP units, as shown at Figs. 6 to 9.

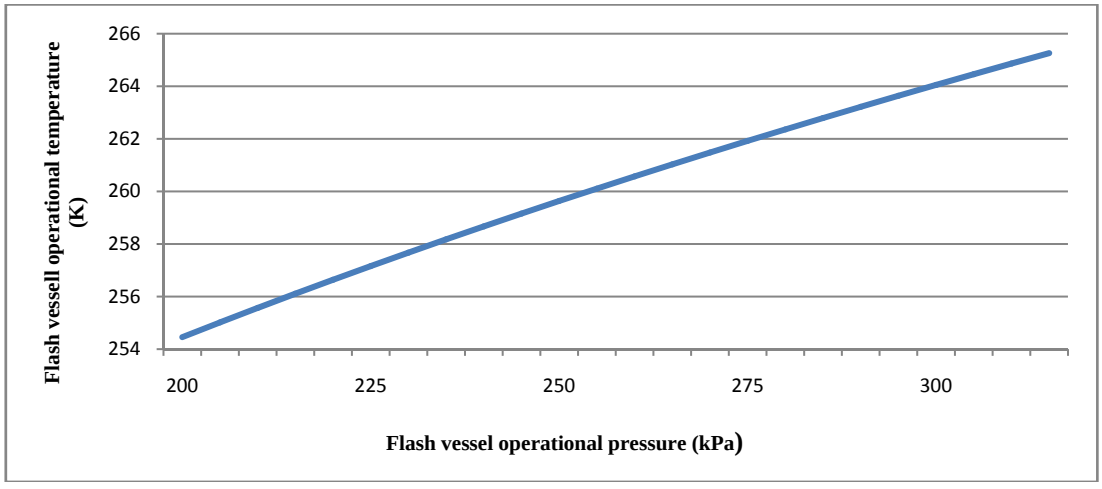

Fig. 3. Pressure influence on operating temperature of the flash vessel

Copyright © 2014 Praise Worthy Prize S.r.l. - All rights reserved

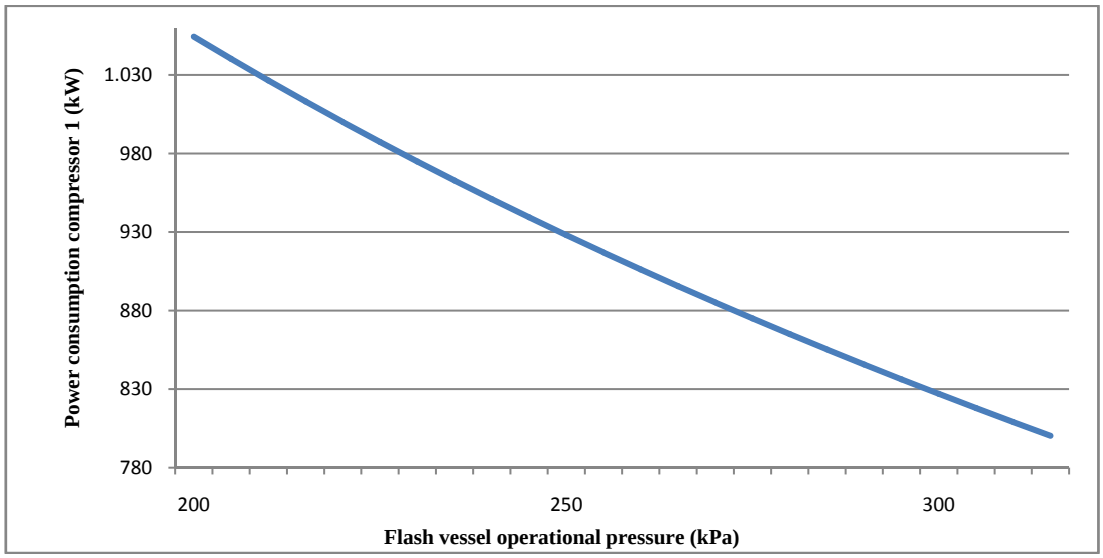

Fig. 4. Flash vessel pressure influence on the power consumption of compressor 1

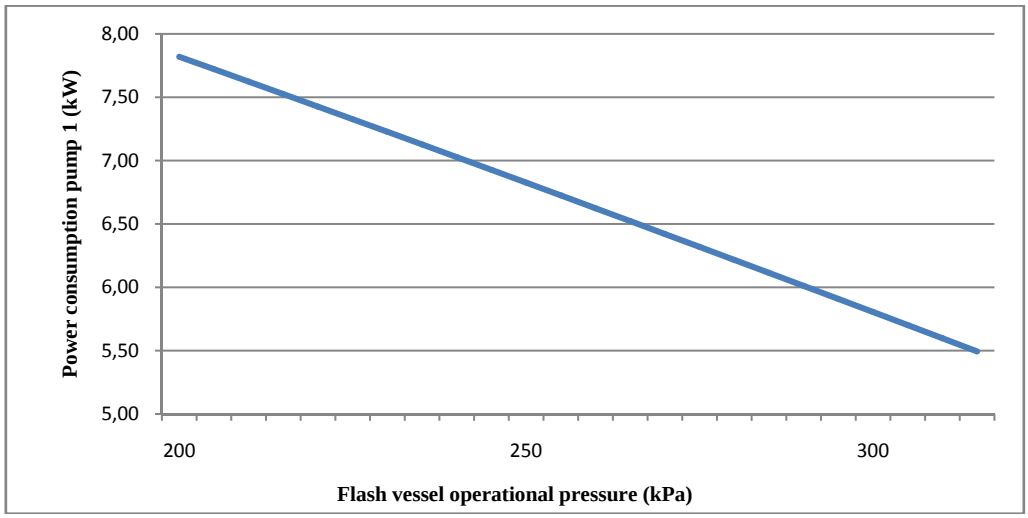

Fig. 5. Flash vessel pressure influence on the power consumption of pump 1

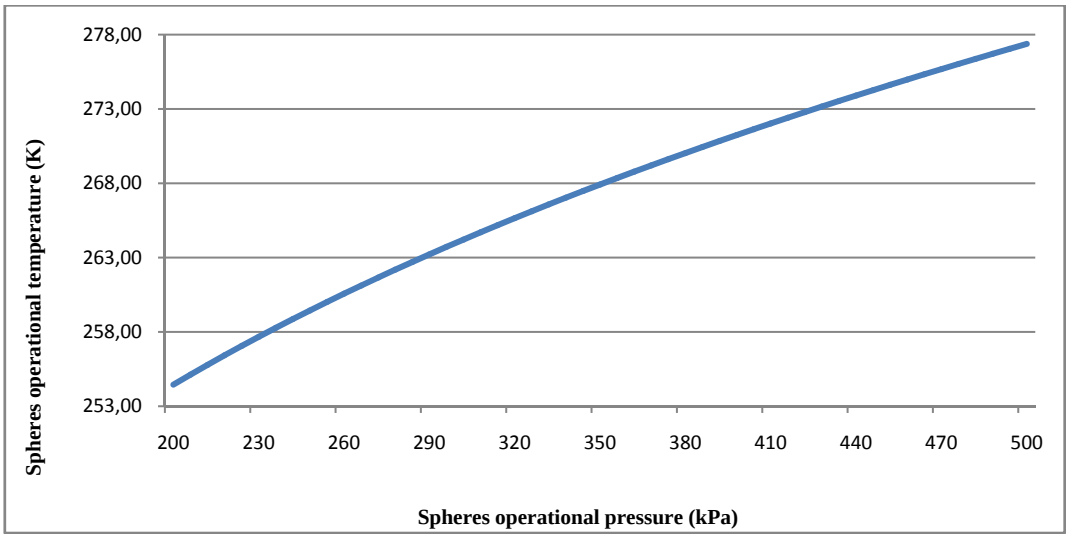

Fig. 6. Pressure influence on the operating temperature of the spheres

Copyright © 2014 Praise Worthy Prize S.r.l. - All rights reserved

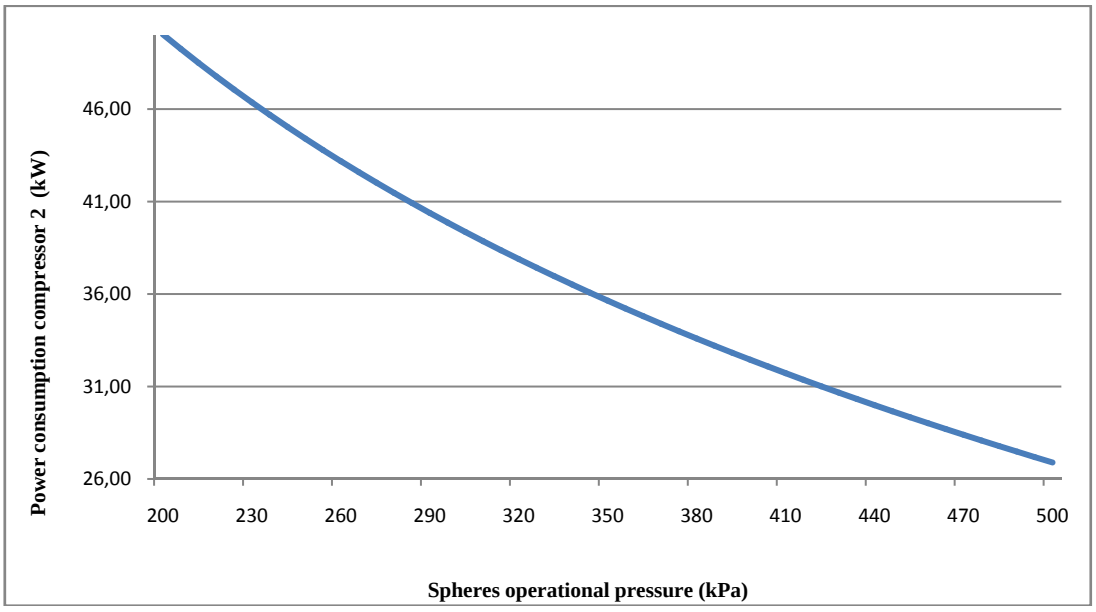

Fig. 7. Influence of the spheres pressure on the power consumption of compressor 2

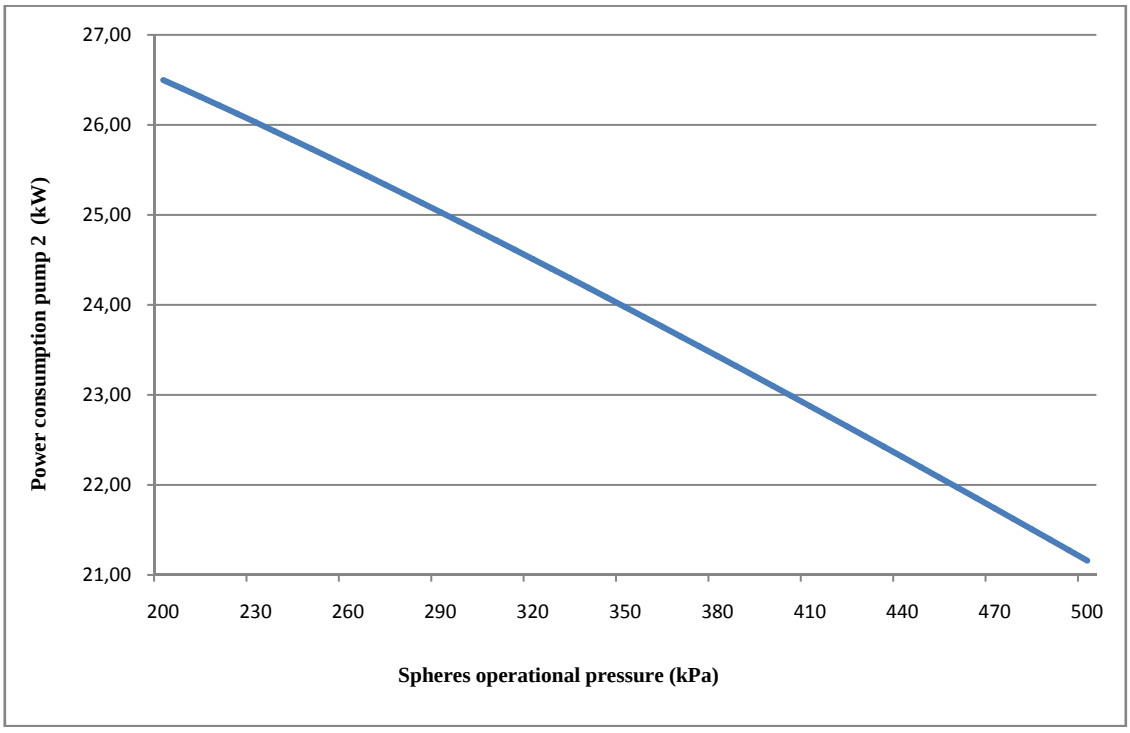

Fig. 8. Influence of the spheres pressure on the power consumption of pump 2

The influence of the operating pressure on the temperature of the spheres has the same reason as the flash vessel. The spheres operate at vapor-liquid equilibrium, at a determined pressure and its saturation temperature. Once more, it is observed that, the higher the operational pressure of the spheres and their outlet streams, the lower the energy consumption of pump and compressor 2, for the same reason detailed at Figs. 4 and 5. From Figure 9, it is possible to observe that, when the operating pressure of the spheres is elevated, the ammonia export temperature to the MAP units increases.

This occurs because, when the operating pressures of the spheres are higher, the temperatures of their outlet streams are higher as well. The spheres liquid outlet streams go to pump 2. The higher the temperature of the pump inlet stream, the higher the temperature of its outlet stream. Although the increase of the operating pressure of the spheres has advantages in the energy consumption of pumps and compressors, the elevation in the ammonia export temperature to the MAP has disadvantages.

Fig. 10 shows the correlation between this temperature and the vapor pressure at the same stream.

Copyright © 2014 Praise Worthy Prize S.r.l. - All rights reserved

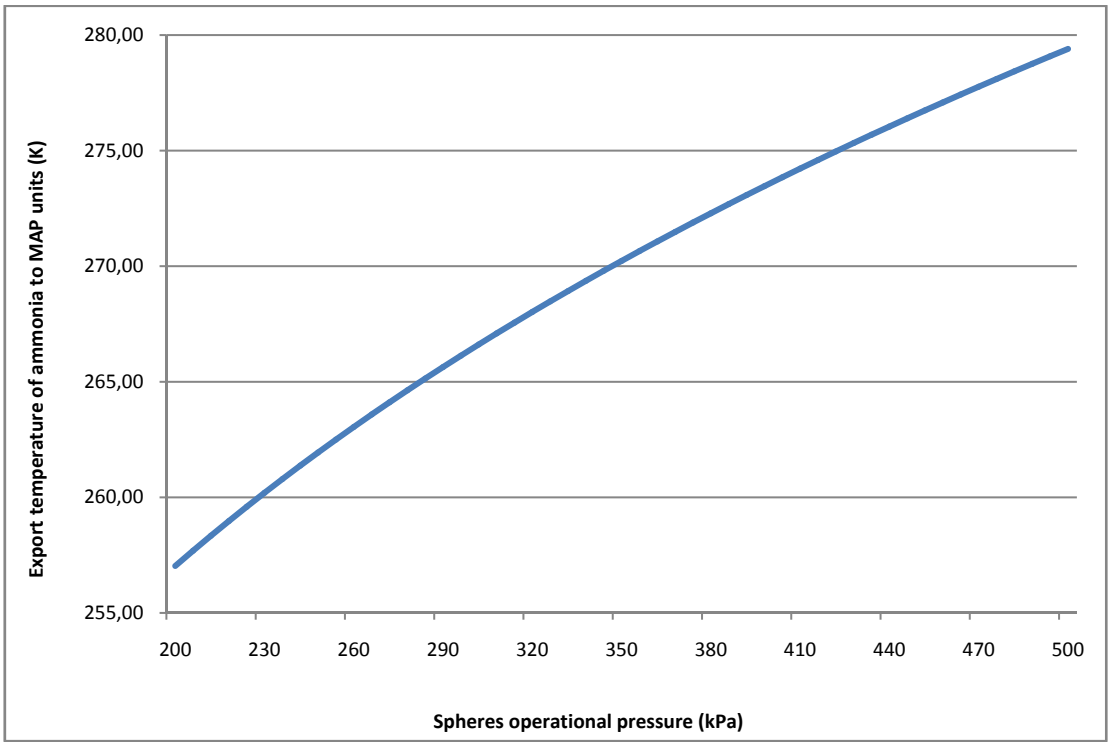

Fig. 9. Influence of the spheres pressure on the ammonia export temperature to MAP units

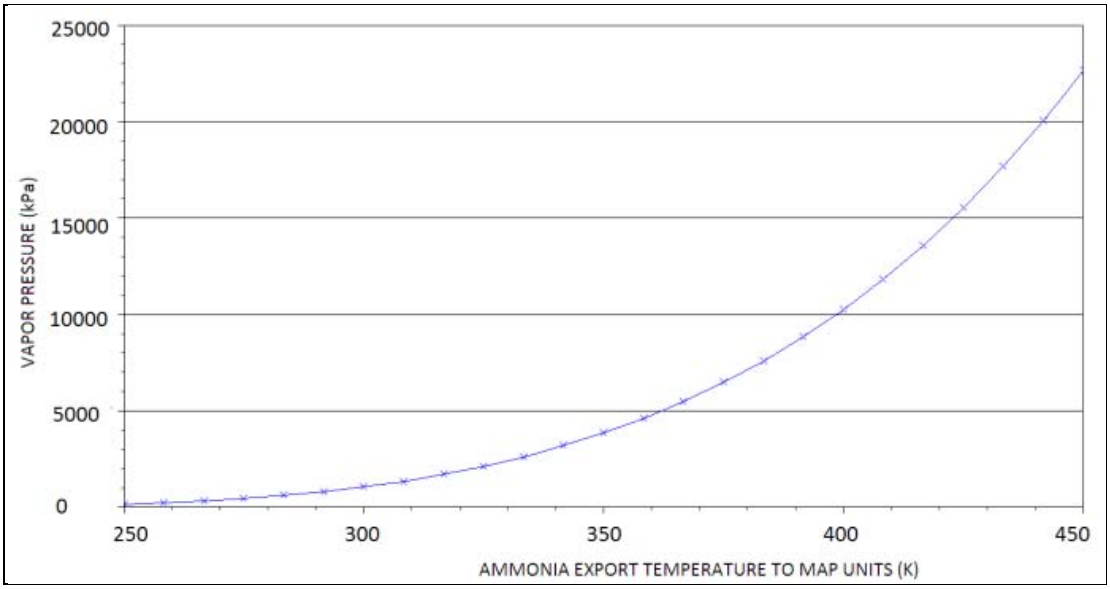

Fig. 10. Influence of the ammonia export temperature to MAP units on the stream vapor pressure

The vapor pressure is the pressure exerted by a vapor when it is in thermodynamic equilibrium with the liquid that gave rise to the system. The system achieves this balance when the rate of vaporized liquid is equal to the rate of condensed vapor. The vapor pressure is a measure of the evaporation tendency of a liquid. The higher its vapor pressure, the higher the volatility, and its tendency to evaporate.

From Fig. 10, it is possible to observe that, the higher the ammonia export temperature, the higher its vapor pressure and its tendency to evaporate. This fact has negative consequences on the industrial unit. It is usual to observe ammonia volatilization, and when the gas enters the pumps, it causes cavitation. This volatilization is aggravated by the old and inefficient thermal insulation of the pipelines.

IV.4. Proposal of a New Adjusted Operational Point

The proposal of a new adjusted operational point took into consideration the following premises: the pressure of the truck does not have influence on the other process

Copyright © 2014 Praise Worthy Prize S.r.l. - All rights reserved

variables; the increase of the flash vessel operational pressure has a positive impact on the energy consumptions of pump and compressor 1; and the increase of the spheres operational pressure has a negative impact on the ammonia export temperature to the MAP units. Considering this points, at the proposed scenario, the truck´s pressure was kept at the current status. The operating pressure of the flash vessel was elevated once more up to 338.32kPa. The elevation was not superior due to the safety of the equipment.

The operating pressure of the spheres was returned to its projected value. The results of this simulation scenarios are shown at Table IV.

TABLE IV
COMPARISON BETWEEN SIMULATED SCENARIOS

	Original design	Current operation	Proposed operation
P flash vessel(kPa)	281.44	318.71	338.32
T flash vessel (K)	262.49	265.54	267.06
P spheres (kPa)	289.29	367.74	289.29
T spheres (K)	263.16	269.19	263.16
Energy consumption compressor 1 (kW)	797.24	793.94	761.46
Energy consumption pump 1 (kW)	6.18	5.42	5.01
Energy consumption compressor 2 (kW)	37.30	34.41	37.30
Energy consumption pump 2 (kW)	25.04	23.65	25.04
Ammonia export T MAP (K)	263.47	269.47	263.47

From Table IV is possible to observe that the proposed operational condition reduces even more the energy consumptions of compressor and pump 1, when compared to both original design and current operational scenarios.

The proposed scenario elevates the energy consumptions of compressor and pump 2 back to their original value, but reduces the ammonia export temperature to the MAP units, which is highly positive to the industrial unit. The overall gain of the proposed scenario is estimated in 36.95kW when compared to the design data and 28.61kW when compared to the current operational point of the industrial unit. One additional gain is the reduction of the ammonia export temperature, which is expected to reduce the volatilization and the pumps cavitation issues.

V. Conclusion

From the results shown at this work, it was possible to verify that COCO chemical process simulator could reproduce very well both design conditions and current operational conditions of an ammonia storage unity.

The best thermodynamic package for ammonia was found to be the equation of state of Peng Robinson.

Using current operational conditions of the unit as reference, parametric analysis was used to prove that the specification of the received ammonia does not have any influence on the other process variables of the industrial unit. On the other hand, the elevation of the operational pressure of the storage spheres increases the temperature of the ammonia exported to the MAP facilities in 6K.

This elevation increases the ammonia's vapor pressure, its tendency to volatilize and causes pump cavitation. Through simulation, a new operational point was proposed. It can be possible to obtain an energetic gain of 28.61 kW at the pumps and compressors when comparing to the current operational point.

This gain corresponds to an energy cost reduction of 3.34% in this equipment. Under this new condition, the temperature of the ammonia sent to the MAP units can be returned to its original design values.

References

[1] Bertucco, A. The Role of Process Simulation in Sustainable Industrial Development. In: Expert Group Meeting on: "Process Simulation and Sustainable Industrial Development: Present State-of-the-Art". November 29- December 1st, 2004. San Marino, Italy.

[2] Coco Simulator. CAPE-OPEN to CAPE-OPEN simulation environment. Available at <http://www.cocosimulator.org>. Accessed in February 26th, 2012.

[3] Co-LaN. The CAPE-OPEN Laboratories Network. Available at <http://www.colan.org>. Accessed in February 26th, 2012.

[4] Fertilizer Company. Process Flow Diagram, Ammonia Storage and Transference. 2006

[5] Fertilizer Company. Operational Reports of the Ammonia Storage Unit. 2013.

[6] Fenghour, A.; Wakeham, W.A.; Vesovic, V.; Watson, J.T.R.; Millat, J.; Vogel, E. The Viscosity of Ammonia. The Journal of Physical Chemistry, v. 24, n. 5, p. 1649-1667, 1995.

[7] Lele, G.S. Ammonia Storage: Selection and Safety Issues. Chemical Industry Digest, p. 85-90, May 2008.

[8] Moran, M.J.; Shapiro, H.N. Fundamentals of Engineering Thermodynamics, Fifth Edition. England, John Wiley & Sons, Inc., 2006. 832 p.

[9] Peters, M.S.; Timmerhaus, K.D.; West, R.E. Plant Design and Economics for Chemical Engineers, Fifth Edition. Boston , McGraw Hill Publishing, 2003. 988 p.

[10] United Nations Industrial Development Organization – UNIDO; International Fertilizer Development Center – IFDC. Fertilizer Manual. Muscle Shoals, AL, USA, Kluwer Academic Publishers, 1998. 616 p.

[11] Van Baten, J.; Szczepanski, R. A Thermodynamic Equilibrium Reactor Model as a CAPE-OPEN Unit Operation. The Journal of Computers and Chemical Engineering, v. 35, p. 1251-1256, 2010.

Authors' information

Federal Universiy of Uberlândia,
School of Chemical Engineering,
Uberlândia,
Brazil.
E-mail: ajassis@ufu.br

Copyright © 2014 Praise Worthy Prize S.r.l. - All rights reserved

2035-1763(201407)6:4;1-2

Copyright © 2014 Praise Worthy Prize S.r.l. - All rights reserved